Celsr1a is essential for tissue homeostasis and onset of aging phenotypes in the zebrafish.

Chunmei Li[1], Carrie Barton[2], Katrin Henke[1], Jake Daane[1], Joana Caetano-Lopes[1], Robert Tanguay[2], and Matthew P. Harris[1]

[1]Department of Genetics, Harvard Medical School; Department of Orthopedics, Boston Children's Hospital, Boston MA.

[2]Department of Environmental and Molecular Toxicology; Oregon State University; Sinnhuber Aquatic Research Laboratory, Corvallis, OR

Short title: Novel factor regulating zebrafish aging

Key words: Aging, progeria, *celsr1*, planar cell polarity, caloric restriction

SUMMARY

The use of experimental genetics has been invaluable in defining the complex mechanisms by which aging and longevity are regulated. Zebrafish, while a prominent model for understanding the genetic basis of vertebrate development, have not been used systematically to address questions of how and why we age. In a mutagenesis screen focusing on late developmental phenotypes, we identified a new mutant, *fruehrentner*, that displays typical signs of aging already at young adult stages. We find that the phenotype is due to loss-of-function in the non-classical *cadherin EGF LAG seven-pass G-type receptor 1a* (*celsr1a*). The premature aging phenotype is not associated with increased cellular senescence or decreased telomere length but is a result of a broad failure to maintain progenitor cell populations in tissues. Through the analysis of a knockin reporter line, we find that *celsr1a*^{GFP} is expressed broadly in early development but becomes restricted during maturation. We show that *celsr1a* is essential for maintenance of stem cell progenitors and leads to shifts in cell fate determination. Although *celsr1a* has many signaling functions including establishment of polarity within tissues, we show that caloric restriction can ameliorate the effect of *celsr1a* on lifespan in part through compensatory upregulation of *celsr1* paralogues. These data suggest that *celsr1a* function helps to mediate stem cell maintenance during maturation and homeostasis of tissues and thus regulates the onset or expressivity of aging phenotypes.

INTRODUCTION

Aging can be viewed as the progressive degeneration of tissue and physiological homeostasis through time. The regulation of aging is complex as it integrates environment, lifestyle, and genetic architecture to maintain homeostasis. However, aspects of aging have clear phylogenetic basis, both in the maximum lifespan as well as the expressivity of aging traits. Although evolution has shaped the manifestation of aging in different animals, there are clearly characteristics and mechanisms shared even between humans and yeast (Bishop and Guarente, 2007; Kenyon, 2010; Vijg and Suh, 2005). These common foundations have allowed the use of experimental laboratory and natural populations to investigate how and why we age. Unbiased genetic screens in Baker's yeast *Saccharomyces*, the nematode *Caenorhabditis elegans*, and the fruitfly *Drosophila melanogaster* have been instrumental in illuminating the genetic and biochemical aspects of aging. Similar unbiased approaches in the mouse have been limited, in part because of the restricted number of progeny produced as well as the fact that mice have lifespans which restricts a systematic analysis of the mechanisms of aging from forward genetic approaches. However, through direct analysis of pathways identified in invertebrate and yeast models, the mouse has functioned as a key experimental system to identify shared aspects of aging and to understand modifiers of aging mechanisms through both environmental and genetic perturbations. Identification of alternative vertebrate models that can leverage the tools of forward genetics would be valuable to identify vertebrate specific regulators of this process.

Fish have long served as important models in the study of aging and lifespan. In particular, guppies have served as a natural and laboratory accessible model to address the causes and evolutionary shaping of senescence (Bronikowski and Promislow, 2005; Reznick et al., 2006; Reznick et al., 2004). Guppies, however, are not well suited for forward genetic approaches leading to the need for other models for use in the laboratory. Zebrafish and medaka have been workhorse models for developmental genetics, however the use of these species to address aging has been limited (Keller and Murtha, 2004). Through reverse genetic approaches, studies have shown that zebrafish share telomere-mediated senescent programs and phenotypes of aging similar to that seen in other animals (Anchelin et al., 2013; Carneiro et al., 2016; Henriques et al., 2013). The phenotypic spectrum includes loss of tissue homeostasis, reduction in fecundity and fertility, kyphosis and shortened lifespan. Following, *lamin A* variants associated with aging-like phenotypes in Hutchinson Gilford progeria have been specifically tested in zebrafish and show analogous phenotypes to human patients (Koshimizu et al., 2011). Similar loss-of-function experiments on medaka have not been carried out, although telomerase

has been shown to be associated with senescent phenotypes (Hatakeyama et al., 2008; Hatakeyama et al., 2016), suggesting that this fish can support genetic analysis of senescence as well. These papers set the foundation for use of small laboratory fishes to study the genetic regulation of aging as they demonstrate shared phenotypic outcomes of known genetic regulators of aging. However, unlike invertebrate genetic models of aging, zebrafish and medaka are not particularly short lived, limiting efficient analysis of lifespan-extending changes. Leveraging the ability to process large numbers of larval zebrafish, Kishi et al performed one of the first unbiased screens in zebrafish to identify genes associated with senescence using expression of SA-β-gal as a biomarker (Kishi et al., 2008). This study is unique in approach, though specifically targets defects in tissue integrity observed in early larvae. As such, it remains unclear if these mutants are representative of the loci regulating normal aging.

The killifish *Nothobranchius furzeri* has become a model to understand the causes of vertebrate aging (Genade et al., 2005; Hu and Brunet, 2018). The utility of this fish model has been due in part to their short lifespan, but they share experimental accessibility of early development thus allowing the study of gene function (Valenzano et al., 2011). As a proof of concept, Harel et al (Harel et al., 2015) show experimental alteration of *telomerase reverse transcriptase (tert)* in *N. furzeri* had comparable senescence phenotypes as seen in zebrafish and the mouse. Although within strain variation in longevity and aging phenotypes are being addressed through genetic mapping (Cui et al., 2019; Kirschner et al., 2012; Terzibasi et al., 2007), to date this model has not been use in broader forward genetic approaches that have been the strength of prior work in other species to uncover how aging and longevity is encoded and can vary.

Here, we report on a novel zebrafish mutant identified through a forward genetic screen for adult phenotypes that exhibit traits in early adulthood that closely resemble those associated with normal aging. The mutant does not show evidence of increased age-associated cellular senescence, but rather is deficient in maintaining tissue integrity through support of stem cell maintenance and proliferation. The phenotype is caused by loss-of-function mutations in the non-classical cadherin, *cadherin EGF LAG seven-pass G-type receptor 1a* (*celsr1a)*. We observe a general loss of proliferative phenotypes in tissues suggesting that the progeric defect seen in mutant is associated with loss of homeostasis in adult tissues. Following we find that the function of *celsr1a* is necessary for the expression of stem cell factors in different tissues. These results suggest that *celsr1a* is linked to stem cell maintenance and/or proliferation and that disruption of its function leads to premature aging phenotypes in zebrafish. Concordantly, we find that *celsr1a* expression wanes in mature fish and coincides with the onset of normal aging. Affirming the role of *celsr1a* in aging programs, we show that caloric restriction can alleviate reduced viability and tissue level pathologies associated with

celsr1a loss, in part through upregulation of *celsr1* paralogues. The identification of a zebrafish model for regulation of stem cell maintenance in aging opens up new avenues for aging research using zebrafish as a genetic tool for discovery.

RESULTS

The identification of an adult zebrafish mutant with precocious geriatric phenotypes

In a large-scale screen for mutations affecting late development of the zebrafish, we isolated a class of mutants having altered scale patterning phenotypes and kyphosis in 10-12 week old adults (wpf, weeks post fertilization). These mutants displayed a broad collection of phenotypes that became more severe with age and resembled normal aging in zebrafish (**Fig. 1**). We focused on one of these mutants, named *fruehrentner (frnt)*, or 'early retiree' in German. The cumulative phenotypic effects from the mutation lead to a progressive decrease in lifespan, with about half of mutant progeny dying before 9-10 months of age (**Fig. 1D**). Fish living beyond this point showed progressive deterioration of their appearance and manifestation of sensorial neural defects causing them to swim erratically and in circles when presented with an acoustic stimulus (**Suppl. movie 1**). Broadly these phenotypes resembled normal aging in wild-type zebrafish, however were apparent during early adult stages. Importantly, the *frnt* mutant exhibited no apparent outward morphological phenotypes as larvae or in juvenile stages. Instead, the observed phenotypes were acquired and only appear in early adults (**Fig. 2**).

Histological analysis of young *frnt* mutant zebrafish and wild-type controls showed clear homeostasis defects in several tissues (**Fig. 2**). In zebrafish, muscle fiber type is segregated in the trunk into a peripheral domain of slow muscle overlying fast muscle fibers (**Suppl. Fig. S1**, **Fig. 2A**). In *frnt*, the fibers of the slow muscle are severely affected and have smaller fiber size and hyperproliferation of mitochondria (**Fig. 2C, Suppl. Fig S1**), many of which are degenerating (**Suppl. Fig. S1G**). An effect of the *frnt* mutation on fast muscle fibers was not apparent. Histological analysis of aged wild-type fish shows comparable thinning of slow muscle fiber thickness as well as fibrosis of the surrounding tissue (**Fig. 2B**). The *frnt* mutant also shows striking defects in the structure of the epidermis (**Fig. 2D-F**). The epidermis of the adult zebrafish integument is a stratified epithelium with prominent cuboidal basal cells (**Fig. 2D**). *frnt* mutants of comparable age show a drastic thinning of the epidermis with fewer basal cells and lengthened squamous cells overlying a thickened dermis (**Fig. 2F**). A similar epidermal thinning and cellular structure is observed in old wild-type zebrafish (>2.5 years; **Fig. 2E**).

These results suggest that the *frnt* mutant affects tissues with high metabolic activity, such as the skin and slow muscle, and is reminiscent of phenotypes observed during normal aging in zebrafish.

The histological characteristics, such as sarcopenia and diminished basal cells of the epidermis, suggest that progenitor cell deficiencies may underlie these pathologies. Supporting this hypothesis, we found that expression of *pax7a*, a marker for muscle satellite cells (Berberoglu et al., 2017; Seale et al., 2000), was decreased in *frnt* slow muscle whereas analysis of a more general cell proliferation marker, *cdnk1a*/*p21,* did not show significant changes (**Fig. 2G,H**). Following, we also assessed expression of *ΔNp63*, which marks potential stem cells of the skin (Guzman et al., 2013; Keyes et al., 2005), as well as the epidermal tight junction marker *claudin-b* as a control in epidermis. We observed a similar decrease in expression in the *frnt* mutant specifically for *ΔNp63* but not *claudin-b* (**Fig. 2J, K**). Thus, the acquired senescent phenotypes observed in the *frnt* mutant coincide with a decrease in progenitor cell markers in these tissues.

The effect of frnt manifests late in development

We extended our analysis of the *frnt* mutant phenotype to ask when in development we were able to detect the onset of phenotypes observed in mature fish. Through histological analysis, we measured the development and maintenance of slow muscle through juvenile development. At 3 weeks of age, both *frnt* mutants and siblings have comparable slow muscle fiber diameter (**Fig. 2I**). However, at 3 and 9 months of development, fiber size in *frnt* mutants is substantially smaller than in their wild-type siblings. This size difference is due to the decreased capacity of fibers to increase in size after 3 weeks of development (**Fig. 2I**). Additionally, we used histological analysis of DAPI stained sections to identify changes in basal cell number in the developing zebrafish epidermis (**Fig. 2L**). At 3 months of age there is little difference in basal cell number between *frnt* mutant and wild-type sibling controls. However, at 9 months *frnt* is deficient in the number of basal cells compared with age matched controls. Thus, similar to slow muscle fibers, the *frnt* phenotype in skin is associated with a failure to increase in cell number. These results suggest that the *frnt* phenotypes manifest during late development, increase in severity with progressive age and affect proliferative/growth potential of maturing tissues.

The frnt phenotype does not stem from increased senescence

Cellular senescence is thought to be one factor regulating homeostasis and onset of aging within tissues (Collado et al., 2007). Hallmark phenotypes of senescence are loss of telomere length as well

as activity of lysosomal β -galactosidase, commonly referred to as senescence-associated β-galactosidase (SA-β-gal) (Lee et al., 2006) (Dimri et al., 1995). Telomeres act as essential regulators of genomic stability that allow for fidelity in genome replication. In each replication of chromosomes, telomere length is maintained by a specialized molecular complex, shelterin, through action of the *tert* gene product.

To understand if senescence was an underlying basis of the *frnt* phenotype, we first looked at total telomere length in mutant zebrafish tissue by Southern blot (**Fig. 3**). For a positive control, we analyzed telomere length in first generation *tert* homozygous mutants, as these mutants have been shown to exhibit late age-related phenotypes and accumulation of senescent biomarkers (Anchelin et al., 2013; Henriques et al., 2013). Southern blots from 1 year-old *tert* mutant tissues show a distinct reduction of average telomere length. In contrast, age matched *frnt* mutants do not show an appreciable change compared to wild-type fish (**Fig. 3A**). We further analyzed the activity of SA-β-gal in histological sections of *frnt*, *tert* mutants and age-matched wild-type tissues as a measure of senescence. Compared to heterozygous siblings, *tert* homozygous mutants show considerable activity of SA-β-gal (**Fig. 3B, C**). In contrast, we saw no discernable difference between *frnt* homozygous mutants and wild-type controls (**Fig. 3D, E**). Thus, there is little evidence that the *frnt* phenotype is due to activated senescence programs typically observed in *tert* deficiencies.

Identification of the genetic cause of frnt aging phenotypes

To identify the genetic locus affected in the *frnt* mutant, we used whole genome sequencing and mapping based on homozygosity-by-descent (Bowen et al., 2012). Initial mapping showed tight linkage to chromosome 4 (**Fig. 4A**). Efforts to refine the map interval using polymorphic markers was limited as the linked region fell within a large chromosomal interval showing low heterozygosity and limited recombination (**Fig. 4C, D**). As we had genomic sequence of the whole interval, we were able to define several missense mutations as potential candidate mutations for causing the *frnt* mutant phenotype, however, there were too many mutations to functionally address. Thus, we performed a non-complementation screen to identify further alleles of *frnt* to define the affected gene. First, using N-ethyl-N-nitrosourea (ENU) induced mutagenesis of wild-type zebrafish, we identified a mutant (*mh36*) within progeny from crosses to *frnt* homozygous fish that failed to complement *frnt.* Sequencing the exome of homozygous *mh36* led to the identification of a nonsense mutation (C1693X) in the gene *celsr1a* within the linked interval of *frnt* (**Fig. 4E**). As chemical mutagenesis can lead to many mutations and the mapping interval was large, we extended this approach by making targeted deletions using CRISPR/Cas9 mediated gene editing in the *frnt* heterozygous background. We were

successful in identifying mutants that exhibited the *frnt* aging phenotype having insertion/deletions predicted to lead to premature truncation of the *celsr1a* gene product (**Fig. 4F).** Following these non-complementation approaches, we reassessed our mapping in the original *frnt* mutant. In depth analysis of the whole genome sequence data of *frnt* mutants at the *celsr1a* gene locus uncovered a unique transposon insertion of approximately 3.5 kb into exon 1 of the *celsr1a* (**Fig. 4G**). The effect of this insertion is predicted to lead to an early truncation of the protein. Thus, through our mapping of *frnt* and non-complementation analysis, we have identified that the *frnt* phenotype is due to a disruption of *celsr1a* function.

Celsr1a is an atypical cadherin of the flamingo family of cadherins. Among vertebrates, there are three ancestral orthologues that are shared, Celsr1-3. Fish have two orthologues of *celsr1, celsr1a* and *celsr1b* (Formstone and Mason, 2005) stemming from a whole genome duplication shared among teleosts. Celsr1a is a large membrane bound protein extending greater than 3000 amino acids in length. The mutations identified all lie in the N-terminal extracellular domain. Given that the mutations cause premature truncations or frameshifts upstream of the first transmembrane domain (**Fig. 4I**), we predict that the *frnt* phenotype is due to loss of *celsr1a* function. The identified alleles all have comparable phenotypes and fail to complement each other, supporting the identified mutants as *celsr1a* nulls. Analysis of the Celsr1 protein by Western blot suggests that the *frnt* allele leads to lack of high molecular weight products and further supports our prediction of loss of *celsr1a* function (**Fig. 4H**).

celsr1a expression wanes with age

Analysis by whole mount *in situ* hybridization has previously shown *celsr1a* to be broadly expressed during gastrulation and early larval development (Carreira-Barbosa et al., 2009; Formstone and Mason, 2005; Harty et al., 2015)(https://zfin.org). To better understand how *celsr1a* functions to regulate the acquired phenotypes seen in the mutant, we used quantitative RT-PCR (qRT-PCR) to assess levels of *celsr1a* expression through development and into adult stages. We find that *celsr1a* is expressed throughout early development and into juvenile stages (30 dpf), at which point expression levels in multiple tissues start to wane and are virtually undetectable in late adult stages (**Fig. 5A**). To better assess differential expression of *celsr1a* during development, we used CRISPR/Cas9-mediated homology directed repair to knockin a *green florescent protein (GFP*) coding sequence into the endogenous *celsr1a* locus. We isolated an expressing line with insertion of GFP 114 nucleotides upstream of the translation initiation site in the 5' UTR of *celsr1a* (**Fig. 5B**). As the insertion allele fails to complement *frnt,* we predict that the allele is disruptive of normal *celsr1a* regulation and function. The identified line, *celsr1a*^{GFP}, recapitulates early expression seen by whole mount *in situ*

(1dpf, **Fig. 5C**), and strongly labels the eye, the central nervous system, the lateral line, the mesonephros and the intestine in young larvae (4dpf, **Fig. 5D**). On close inspection, *celsr1a*^{GFP} is expressed, albeit at lower levels, in both epidermis and slow muscle (**Fig. 5E-F,H**). These tissues show strong pathologies in the mutants (**Fig. 2**). Notably, only select cells are labeled in the early epidermis, suggesting differential expression of *celsr1a* within this tissue (**Fig. 5E**). At 12dpf, *celsr1a* expression remains prominent in slow muscle fibers, (**Fig. 5H** and data not shown) and in the intestinal epithelium (**Fig. 5I, J**). Similar to findings by Hardy et al, (Harty et al., 2015) and our qRT-PCR results (**Fig. 5A**), we find that *celsr1a* expression wanes in late development, with higher expression in young juveniles and limited expression as adults. Expression of *celsr1a* in adults is retained primarily in neuromasts and with a low expression level throughout other tissues.

celsr1a is required for polarity of integumentary appendages

Celsr1 is a key component of planar cell polarity (PCP). In concert with Frizzled, Van Gogh (Vang), and non-canonical Wnt signaling factors, Celsr1 regulates cell asymmetry and developmental signaling pathways (Goffinet and Tissir, 2017; Tissir and Goffinet, 2013). The role for the other orthologues, *celsr2* and *3* is unclear. A Celsr1-deficient mouse has been used to study the role of PCP in development. Homozygous *Celsr1* mice show pelage phenotypes with misaligned hair follicles and the appearance of whirls (Devenport and Fuchs, 2008; Ravni et al., 2009). A similar phenotype is also seen in the patterned arrays of tongue papillae in Celsr1 deficient mice (Wang et al., 2016). Both phenotypes are also observed in mice with alterations in *Vang2* gene function (Devenport and Fuchs, 2008; Wang et al., 2016) and are considered reliable readouts of PCP signaling in adult mice.

The role of *celsr1a* in regulating PCP signaling during zebrafish development has not been addressed. Analogous structures to hair of mammals in zebrafish are scales. In contrast to hair, which is primarily an ectodermal derivative, scales in fishes are primarily mesodermal, comprising components of the dermal skeleton. However, scale development is dependent on the formation of an ectodermal placode, a structure homologous to the placodes necessary for other integumentary structures such as hair and feathers (Harris et al., 2008). Thus, early aspects of formation and patterning are conserved between divergent structures of scales and hair, and it has recently been shown that further downstream pattering is similar as well (Aman et al., 2018). Scales form ordered arrays of overlapping surface skeletal elements across the body (**Fig. 6A**, **C**). Within each scale there is an internal polarity, biasing the growth to the caudal aspect of the scale from an initial osteogenic focus (**Fig. 6E**); this polarized accretionary growth leads to the formation of overlapping arrays of scales along the flank of the fish. We investigated scale formation in the zebrafish as biomarkers of altered

PCP signaling in *frnt* mutants. At the earliest timepoints of scale development analyzed, *frnt* mutants had obvious scale patterning defects (~ 8 wpf). These defects are maintained in adults showing spiraling patterns of scales on the flank (**Fig. 6D**). Furthermore, individual scales in *frnt* mutants show radial patterning in stark contrast with the polarized growth of scales from wild-type individuals (**Fig. 6G**). Thus, alteration in *celsr1a* in zebrafish affects the patterning of structures that are analogous to those structures affected in the Celsr1 mouse mutant. These phenotypes are consistent with a role of *celsr1a* in PCP signaling during zebrafish development.

celsr1a is required for proliferative capacity and maintenance of intestinal progenitor cells

One of the more consistent phenotypes in aging is loss of tissue organization and homeostasis as a function of age. Our histological analyses suggest that several tissues in *celsr1a/frnt* mutants are diminished associated with decreased expression of stem cell markers (**Fig. 2**). The intestinal epithelium has served as a fundamental model of how stem cells within a tissue are specified and maintained. However, only few papers have detailed differentiation and stem cell biology and differentiation in the intestine in fishes (Aghaallaei et al., 2016; Lickwar et al., 2017; Wallace et al., 2005; Zhao and Pack, 2017). To investigate the role of *celsr1a* in maintaining tissue homeostasis and progenitor populations in adult tissues, we analyzed changes in the intestinal epithelium in the *frnt* mutant. Consistent with our findings in other tissues, analysis of the histological pathology of the intestine of *frnt* demonstrates a significant decrease in epithelial thickness and a reduction of the anterior gut circumference (**Suppl. Fig. 2A-D**). Histological analyses also indicated changes in differentiation of the epithelium, as more goblet cells were found in the *celsr1a* mutant compared to age matched controls (**Suppl. Fig. 2E-H**).

We find that the mutant phenotype in the intestine is associated with drastic changes in the proliferative capacity of the intestinal epithelium. After short term Bromodeoxyuridine (BrdU) labeling, adult *frnt* mutants showed negligible BrdU incorporation in the intestine compared to age matched controls (**Fig. 7A-D, Suppl. Fig 3A**). Identified BrdU positive cells were found localized near the base of rugae. Consistent with these findings we show reduction of phospho-histone H3 labeling of mitotic cells in rugae (**Suppl. Fig. 3D**). BrdU incorporation in the intestinal epithelium in which *celsr1a* cells are marked with GFP (*celsr1a*^{GFP}) shows restricted incorporation of BrdU into *celsr1a*$^{+}$ cells during growth of heterozygous larval intestine (**Fig. 7J**). This suggests that *celsr1a*-expressing cells in the intestine are not actively cycling. In an effort to address maintenance of progenitor pools in the intestinal epithelium, whole mount *in situ* analysis of potential stem cell markers, such as *sex determining region Y-box 2* (*sox2*) (Kuzmichev et al., 2012; Que et al., 2007)

(Chen et al., 2015) (**Fig. 7E,F**) and *olfactomedin 4* (*olfm4*) (**Fig. 7G-I**) (van der Flier et al., 2009) (Igarashi and Guarente, 2016), were performed in the adult intestine of wild-type and *frnt* mutant fish. Supporting our expression analysis in skin and slow muscle, we detected a strong reduction in *sox2* and *olfm4* positive cells in *celsr1a* mutants, suggesting that *celsr1a* is required for normal maintenance of progenitor cells in the intestinal epithelium.

Celsr1a^{GFP} is expressed in a small subset of cells in the developing intestinal epithelium (**Fig. 5**) resembling enteroendocrine cell (EEC) morphology. *Neuronal differentiation 1* (*neurod1*), is a transcription factor associated with notch signaling, which is a late marker for EECs in the intestine of mice and zebrafish (Li et al., 2011; Lickwar et al., 2017). Using the transgenic line, *Tg(neurod1:TagRFP)*, we found that in early development, *Tg(neurod1:TagRFP)* labels a subset of *celsr1a*^{GFP} positive cells (**Fig. 7K**), suggesting that the function of *celsr1a* may predominate in enteroendocrine cells. As a small number of *celsr1a*-expressing cells were identified without *neurod1* expression, it is likely that *celsr1a* represents an earlier stage in their specification. Mutant intestines are markedly thinner (**Supp Fig 2**) however retain a complement of *celsr1a*-expressing cells (**Fig. 7J**).

One hallmark of resting stem cells is their slow cycling during normal tissue homeostasis. To further determine the effect of loss of *celsr1a* function on proliferative capacity, we assessed the retention of BrdU at extended chase periods to permit detection of slower cycling cells. Analysis of single nucleoside dosing events over 48 hours indicated a progressive reduction of differences between mutants and siblings in the cells retaining or incorporating BrdU label in the intestine (**Supp Fig. 3**). These data suggest that existing progenitor populations are retained in the *celsr1a* mutant and are able to proliferate at these late stages in a limited capacity.

Effect of caloric restriction on celsr1a phenotypes.

The phenotypes we observed in *celsr1a* deficient animals resemble the anatomical and behavioral aspects of normal aging in wild-type zebrafish. To assess the role of *celsr1a* in mediating aging processes, we wanted to analyze how alteration in mechanisms previously related with progression of aging phenotypes would affect *celsr1a* mutant phenotypes. Caloric and dietary restriction are two commonly used strategies that have been shown across animals to have a consistent protective effect on the manifestation of aging phenotypes (Fontana and Partridge, 2015; Speakman and Mitchell, 2011). The regulation of these effects on reducing aging phenotypes is thought to be in part through the action of the Sirtuin family of acetyltransferases (Guarente, 2013), mTOR (Blagosklonny, 2010) and Insulin receptor/Foxo signaling (Kim et al., 2015; Mouchiroud et al., 2013). In fish models, the effects of dietary restriction on aging and age-related pathologies have been mainly tested in zebrafish,

in which most studies use overall dietary restriction as means of nutritional regulation (Adams and Kafaligonul, 2018; Arslan-Ergul et al., 2016; Novak et al., 2005). Such treatment regimens have shown changes in age-related neurological and behavioral phenotypes (Adams and Kafaligonul, 2018) and can have long term impacts on maintenance of weight and health of the fish (Arslan-Ergul et al., 2016). Caloric restriction (CR) regimens have been tested in zebrafish, however the outcomes on age-related phenotypes have not been reported (Robison et al., 2008). Although dietary restriction has the potential to alleviate age-related phenotypes, the extent by which this regulation operates in fishes remains an open question.

We set out to test if modulation of caloric restriction would attenuate the pathology observed in *celsr1a* mutant fish. Simply restricting access to nutrition through a short term limited feeding regimen (*e.g* (Arslan-Ergul et al., 2016) led to decreased fish vitality and viability and was not continued. In order to avoid malnutrition, we designed unique feeds that limit the total caloric content of the food without reducing the lipid and vitamins/minerals (**Suppl. Table 1**). Observations showed that adult fish actively fed on all experimental feeds. Two separate replicate experiments were set up. In each, an equal number of young adult fish of particular genotypes were grouped into common feeding populations. In the first experiment, wild-type fish were compared to homozygous mutants (n=17), whereas in the second experiment *frnt* siblings (i.e. +/+ and +/-) were compared (n=30). Over the course of the experiment, there was no significant reduction in weight in the different feeding groups, however there was a marked lack of increase in body mass in the 50% restricted feeding group (**Fig. 8C**).

Zebrafish fed with control feed followed the general expectation for the zebrafish lifespan, with greater than 70% survival over a 5 month period (**Fig. 8A**). *Frnt* sibling controls (wild-type and heterozygous mutants) however, provided with the same feed showed a considerable shift in viability (**Fig. 8B**), suggesting a potential dominant effect of *celsr1a* on long-term viability. In both experiments, 25% reduction in calories did not show any significant effect on viability in wild-type, sibling controls or *frnt* mutants (**Fig. 8A, B**). However, in 50% calorie reduced groups, both homozygous *celsr1a* mutants as well as control groups showed a significant shift in lifespan (**Fig. 8A, B**).

As viability is a broad assessment of potential changes in aging, we looked closely at changes in phenotypes associated with loss of *celsr1a* function in mutants fed different diets. As feeding regimens were initiated in 3 month-old fish sorted by their integumentary phenotypes, scale phenotypes were found in all treated fish as they were already present at the start of feeding. Therefore, this phenotype cannot be used to assess response to CR. Instead, we used behavior as a

measure of change in aging-related degenerative phenotypes (**Fig. 8D**, **Suppl. movie 2**). We found that 50% reduced caloric intake results in a considerable reduction in the circling behavior and sharp turns observed in *celsr1a* mutants (**Fig. 8E-F**), suggesting that the treatment halted or ameliorated this phenotype in the mutant. Although behavior and lifespan significantly improved with 50% reduction of calorie intake, overall morphology of the *frnt* mutant survivors remained unaffected (**Suppl. Fig 4**).

Compensatory effects in response to caloric restriction

As a means to understand changes in known metabolic regulators in response to caloric restriction, we assessed expression changes in *sirtuins* and *cdkn1a*/*p21* in surviving fish from the different treatment strategies. We found an upregulation of *sirt1*, *sirt6* and *cdkn1a/p21* expression in adult calorie restricted fish in both siblings and *celsr1a* mutants, when compared to fish fed control diets (**Fig. 8G-J**). As previously noted, *celsr1* in the zebrafish has two paralogues, *celsr1a* and *celsr1b* as well as two orthologues, *celsr2* and *celsr3*. Intriguingly, in both siblings and homozygous *celsr1a* mutant fish, caloric restriction led to an increase in *celsr1b* expression (**Fig. 9A, B**). A significant increase in expression of *celsr2* or *celsr3* orthologues can be seen in siblings treated with 50% CR feed. Paralleling these data, in the surviving *frnt* mutants an upward trend in *celsr2* or *celsr3* gene expression is also observed (**Fig. 9C, D**). These data suggest that in tandem with an increase in metabolic regulators of aging such as *sirt1* and *cdnk1a*/*p21*, caloric restriction causes an upregulation in *celsr1b* that may contribute to the observed rescue.

DISCUSSION

Zebrafish have served as a highly efficient laboratory model to perform unbiased screening for the genetic regulation of embryonic and post-embryonic development. However, its use towards investigating the regulation of aging has been limited. Here, using a forward genetic approach in the zebrafish centering on phenotypes manifesting in the adult, we isolated a new mutant class which exhibits a collection of phenotypes that together closely resemble natural aging. In a direct comparison between *frnt* mutants with older fish showing outward appearance of senescence, we demonstrate the similarity of the mutant phenotype with normal aging pathologies in fishes. All the phenotypes noted in *frnt* are shared with other vertebrates and are seen in normal and accelerated aging in both mice and humans. Cloning of the zebrafish mutants revealed that the progressive loss of homeostasis was due to mutation in *celsr1a*, a member of the flamingo family of cadherins. Expression of *celsr1a* is found within specific tissues in developing fish and diminishes as fish mature. Thus, the loss of *celsr1a*

function in the *frnt* mutant may reflect conditions occurring at later stages of adult development and homeostasis, leading to the early appearance of aging-like phenotypes.

Conservation of Celsr1 function in vertebrates

Our identification of *celsr1a* giving rise to an adult aging phenotype in the zebrafish is surprising as loss-of-function mouse models and humans carrying mutations in *Celsr1* have a high prevalence of neural tube closure defects (Allache et al., 2012; Chen et al., 2018; Curtin et al., 2003; Murdoch et al., 2014; Robinson et al., 2012; Wang et al., 2018). As other planar cell polarity regulators are associated with neural tube defects and have been shown to genetically interact with Celsr1 to increase the severity of the pathology (Murdoch et al., 2014; Wang et al., 2018), planar cell polarity most likely plays a key role in the etiology of these disorders. We do not see neural tube defects arising in the *frnt* mutants nor do we observe reduced numbers of juvenile *celsr1a* homozygous mutants as would be expected from early lethality. Zebrafish have two paralogues of many genes as a result of an ancestral whole genome duplication. Retention of paralogues can provide redundancy and buffering of essential functions, allowing for resolution of functions later in development. Although we have not specifically investigated the overlapping function of *celsr1* paralogues, such redundancy may be a reason for the lack of early neurulation phenotypes. Another hypothesis for the lack of neural tube defects in *frnt* mutants is simply that zebrafish do not have similar morphogenesis of the neural tube as seen in mammals. In teleosts, the neural tube forms by cavitation of a neural cylinder, the neural keel (Papan and Campos-Ortega, 1994). Prior data suggested that morpholino knockdown of *celsr1a* led to neural keel defects (Formstone and Mason, 2005), however we do not observe these phenotypes in any of the defined *celsr1a* mutants. It is likely that the morphogenesis and intercalation that occurs during neurulation in mammals and is affected by altered *Celsr1* function does not occur in the zebrafish. This early developmental difference in fish may have permitted the discovery of the late developmental effects of *celsr1a* seen here and revealed a role for this gene in the regulation of aging.

Celsr1 plays several signaling roles both in planar cell polarity/ non-canonical Wnt, as well as, Hippo signaling. Mice with deficiencies in Celsr1 show distinct polarity defects in mouse oviduct epithelia (Shi et al., 2014), hair development (Devenport and Fuchs, 2008) (Ravni et al., 2009) as well as patterning of tongue papillae (Wang et al., 2016). We see an analogous phenotype of integumentary phenotypes in the patterning and loss of asymmetry in scales of the zebrafish (**Fig. 6**). Integumentary appendages, while structurally diverse, all share a common early patterning placodal stage, suggesting this may be a point at which pattering is determined by Celsr1. *Celsr1* mutants in the mouse have also

been found to have a dominant effect on vestibular function (Curtin et al., 2003). This has been shown to be associated with misoriented outer hair cell stereociliary bundles regulated by PCP signaling (Curtin et al., 2003). The consequence of these vestibular defects is altered stereotaxis and swirling of mouse Celsr1 mutants (e.g *crash* (*csh*) and *spincycle* (*Scy*)). We show that *celsr1a*-deficient zebrafish show comparable behavioral phenotypes with prominent circling/swirling behavior as seen in the mouse (**Fig. 8 and Suppl. movie 1**). Although a detailed analysis of the vestibular system and otoliths in *frnt* mutants have not been carried out, it is likely that a similar mechanism underlies this phenotype in both species.

<u>*Role of celsr1a in regulating progenitor cell populations*</u>

Although resembling normal aging, *celsr1a* mutant fish do not show significant shifts in expression of senescence biomarkers (**Fig. 3**). However, many tissues show acquired deficiencies in tissue integrity and homeostasis similar to those observed in normal-aging zebrafish. These homeostatic aging phenotypes are coincident with decreased tissue specific markers of resident stem cells and proliferation. Expression analysis shows *celsr1a* diffusely expressed during early embryogenesis becoming localized to a diverse array of tissues as development progresses (**Fig. 5**). Within the intestinal endoderm, *ceslr1a*^{GFP} has heightened expression of the marker in localized basal cells. The majority of cells strongly expressing *celsr1a* co-label with *neurod1* a marker for differentiated EECs suggesting a role of these cells in the observed pathology seen in the mutants (**Fig. 7K**). These cells are not actively cycling as they do not take up BrdU (**Fig. 7J**). Previous work has identified EECs as being a source of quiescent stem cells in the adult mouse intestine (Basak et al., 2017; Sei et al., 2018). EECs are sufficient to contribute to homeostatic and repair activities in the mouse in cell populations not expressing the broad stem cell factor *leucine-rich repeat-containing G-protein coupled receptor 5* (*Lgr5*) suggesting EEC may be a source of resident quiescent stem cells for this tissue. Lgr5^{+} intestinal stem cells show a bias towards differentiation into EEC morphologies *in vitro* suggesting EECs may have developmental potential within the intestine for proliferation and stem cell function (Basak et al., 2017; Buczacki et al., 2013) (Sei et al., 2018). Zebrafish do not have a *Lgr5* orthologue for direct comparison, however we show that *celsr1a* marks a similar population of secretory EECs and that loss of *celsr1a* function leads to a loss of homeostasis and decreased progenitor cell number. Thus, *celsr1a* may be essential for the specification of an early defined EEC population in the zebrafish comparable to those detailed in the mouse having quiescent stem cell properties (Buczacki et al., 2013).

In mice and zebrafish, notch signaling is required for EEC differentiation (Flasse et al., 2013; Fre et al., 2005). Inactivation of notch signaling in the mouse leads to a decrease in stem cell

progenitors and overpopulation of goblet cells in the villi (Jensen et al., 2000; Kokubu et al., 2008; Pellegrinet et al., 2011; Riccio et al., 2008; van Es et al., 2005). A similar phenotype is observed in *celsr1a* mutant zebrafish intestines at adult stages, suggesting that the decrease in proliferative capacity may be due to abnormal differentiation of progenitor cells in the mutant (**Suppl. Fig. 2**). Although, further analysis will have to address if notch signaling is decreased in the condition of *celsr1a* deficiency, evidence from the Drosophila orthologue *flamingo* further supports a mechanistic link between PCP and notch signaling (Le Garrec and Kerszberg, 2008).

The role of *celsr1a* in regulation of adult stem cells may be shared in various tissues. *Celsr1* mRNA is found to be expressed in zones of neural stem cell (NSC) proliferation in the mouse and abates postnatally in parallel to decreasing numbers of NSC (Goffinet and Tissir, 2017). Similarly, *Celsr1* in the mouse was recently found to mark a population of quiescent mesodermal stem cells that contribute to tissue repair (An et al., 2018; Sugimura et al., 2012). Thus, the effects of *celsr1a* deficiency we observe in the intestine, skin and muscle may have broader implications to stem cell regulation in other tissues, consistent with the degenerative, acquired phenotypes we observe in the *celsr1a* mutants. We favor hypotheses of a tissue specific role for *celsr1a* in the regulation of aging phenotypes, however given the role of EECs in hormonal regulation, it remains a possibility that the compound effects and acquired aging phenotypes observed across several tissues in the *frnt* mutant are mediated through systemic/hormonal signaling from the intestine.

A zebrafish model of stem cell regulation and aging.

Phenotypes resembling aging can be influenced by metabolism, activation/alleviation of senescent cell influences, epigenetic regulation such as methylation and acetylation, and general loss of fidelity in transcriptional regulation. Tissue homeostasis is a key factor maintaining tissue vitality and physiological function and has been proposed to be a major factor regulating age-associated phenotypes in many organs and tissues (Liu and Rando, 2011; Schultz and Sinclair, 2016). We identified progeric mutants showing broad tissue level deterioration and loss of proliferative capacity of tissues. Our data suggest that the phenotypes are due to specific loss of progenitor cells in tissues and correlate with loss of stem cell markers such as *dNp63* in the epidermis, *pax7a* in slow muscle, as well as *sox2* and *olfm4* in the intestinal epithelium. The identification of *celsr1a* as a causative factor underlying these phenotypes suggests that PCP signaling is essential for the appropriate maintenance of stem cells in adult tissues. We show that *celsr1a* marks EEC cells in the zebrafish, cells previously defined as having stem like capacity in the mouse intestine. Thus, *frnt* mutants reveal a new model for the regulation of stem cells and association with aging in the zebrafish.

It has been difficult to completely reconcile phenotypic similarities between progeria and normal processes occurring during aging (Burtner and Kennedy, 2010). One way to address this question is to see if treatments thought to suppress normal aging can ameliorate the age-related pathologies observed in mutants. We designed a specific caloric-restricted diet for the zebrafish as a means to test if we could modify the *frnt* aging phenotype through modification of diet. Shifting to a restricted diet in late development showed to be quite efficacious in extending the viability of the mutant, as well as heterozygous siblings specifically in 50% caloric reduced feeds (**Fig. 8**). Caloric restriction also resulted in decreased manifestation of aging phenotypes in *celsr1a* mutants including vestibular function and erratic swimming behavior (**Fig. 8D-F**) as well as an upregulation of markers consistent with metabolic regulation of aging (**Fig. 8G-I**). Interestingly, the effect of caloric restriction led to upregulation of *celsr* paralogues, suggesting that alteration of *celsr* function can compensate in part for *celsr1a* deficiencies. The reduced expressivity of the mutant phenotype by caloric restriction supports that the alterations in the *frnt* mutant cause changes that are normally modulated by pathways associated with normal aging.

CONCLUSIONS

Through use of genetic screens in zebrafish we have identified a new role of *celsr1a* in stem cell function, maintenance and/or proliferation and that disruption of this regulation leads to premature aging of zebrafish. Importantly, the phenotypes detailed occur late in development and affect the early onset or expressivity of aging phenotypes. Although zebrafish are not well suited for systematic analysis of longevity due to their relatively long normal lifespan, one promising aspect of defined mutants having premature aging is their use in screens for genes or specific alleles that can specifically abrogate effects on aging or lifespan phenotypes. Such modifier screens remain a viable future research strategy and tool for discovery using this model. Our work in identifying a novel mutant and characterizing aging phenotypes in the zebrafish, provides a new foundation to investigate aging in vertebrates.

ACKNOWLEDGEMENTS

Work was supported by the Ellison Medical Foundation, and Glenn Foundation awards to MPH and partially supported by grant NIH 2R01DE019837-09 (JTS/MPH). The authors wish to thank expert

help of Dr. Heinz Schwartz and Iris Koch for electron microscopy assistance and Ines Gehring for early positional mapping of the *frnt* mutant.

METHODS:

Husbandry

A complete description of the husbandry and environmental conditions in housing for the fish used in these experiments is available as a collection in protocols.io dx.doi.org/10.17504/protocols.io.mrjc54n. All experimental procedures involving fish conform to AAALAC standards and were approved by institutional IACUC committee. Mutant alleles used in this work are *celsr1a*^{t31786} *(R122Ins3.5kb), celsr1a*^{mh36}*(C1693X), celsr1a*^{mh104}*(P2027A-fs11X), celsr1a*^{GFP} (*mh202*, L74InsGFPfs), and *tert*^{hu3430} (C168X). Transgenic line *Tg(neurod1:TagRFP)* was kindly provided by Dr. John Rawls.

Fish behavior videotaping

Four tanks were placed in a 2x2 stack with each tank housing a single individual (**Suppl movie 2**). Single recordings were made in order to avoid the mis-tracking of individuals. Fish were put into the video tank 10 minutes before recording in order to allow them to acclimate. Behavior was then videotaped for 5 minute periods. Behavior such as the swimming distance, velocity, time spend in the top half of the tank, change in direction (swim changes from one direction to another direction), erratic turn times (fish swirl or rapid direction changes (≥ 2 turn/s)) in the five minutes video were recorded and analyzed by ANYMAZE (Stoelting Co.).

Quantitative polymerase chain reaction

Tissues were isolated and immediately frozen in liquid nitrogen before storing in -80°C or put in TRI Reagent (Sigma) for RNA extraction immediately. Total RNA was extracted by TRI Reagent (Sigma) or Direct-zol RNA Miniprep Kit (Genesee Scientific), and RNA was reverse-transcribed by Superscript IV (Invitrogen) or RNA to cDNA EcoDry Premix (Oligo dT) (Takara). PCR was carried out using QuantiFast SYBR Green PCR Kit (Qiagen) or SYBR Green PCR Master Mix (Applied Biosystems). The expression levels of target genes were normalized to the levels of reference genes, ribosomal protein L13 alpha (*rp113a*) or tubulin (Tang et al., 2007). The relative expression ratio of each target gene to the reference was normalized to the control group ($2^{-\Delta\Delta ct}$ method). All qRT-PCR

assays in a particular experiment were undertaken at the same time under identical conditions and performed in triplicate. Primer sequences used for gene amplification are listed in **Supp table 2**.

Mutagenesis and non-complementation screen

Tuebingen male fish were treated with N-ethyl-N-nitrosourea (ENU; Sigma) following an optimized protocol using clove oil (Sigma) as a sedative (Rohner et al., 2011). The surviving mutagenized founders were crossed to *frnt*^{t31786} homozygous females. Progeny were screened at 2-3 months of age to identify *frnt* phenotypes. Mutants were maintained by out crossing to Tuebingen wild-type strain and incrossing..

Mapping of *frnt*

Rough mapping of the mutant *frnt* was based on a whole genome sequencing method described previously (Bowen et al., 2012). DNA from 20 homozygous F2 from *frnt/+* incrosses was isolated and pooled for DNA library construction. Whole-genome sequencing was carried out on an Illumina HiSeq2000, using 100-bp single-end sequencing. Linkage was confirmed and an interval was narrowed down by analysis of recombinants using microsatellites and SNP markers. To further refine candidate genes, the ENU generated allele (*mh36*) that failed to complement *frnt* was sequenced. DNA was isolated from two homozygous individuals and whole-exome sequencing was carried out using 50-bp paired-end sequencing. Three top candidates which had either missense/nonsense mutations or low coverage in the linked region in both of the alleles were chosen for CRISPR/Cas9 targeted mutagenesis. Sequencing of the non-complementing alleles *frnt*^{t31786} and *frnt*^{mh36} identified *celsr1a* as the likely causative gene in *frnt*^{t31786}. Analysis of whole genome sequencing data identified a sharp break point in the sequencing read coverage of *celsr1a* in *frnt*^{t31786}. To search for reads spanning this insertion, we used Blastn (Altschul et al., 1990) to identify reads where one half of the read had 100% match to either side of the putative insertion. We then used CAP3 (Huang and Madan, 1999) to perform a *de novo* contig assembly on the identified reads. We were unable to assemble a single contig containing the entire insert, suggesting this insert spanned a greater length than could be contained in a single 100bp sequencing read. To identify the identity of the insert, we then performed BLAT on Ensembl against the zebrafish genome on the non-*celsr1a* portion of each contig. Through this, we discovered that the *frnt*^{t31786} mutation was due to a 3.5 kb transposon insertion in exon 1 of *celsr1a* (ENSDARG00000093831). *frnt*^{mh36} had a nonsense mutation in exon 8 of the same gene.

Reverse genetic editing of *celsr1a* locus

Homozygous *frnt*^{t31786} were outcrossed to Tuebingen wild-type fish and progeny *(frnt/+)* were used for complementation testing. Guide RNA (gRNA) targeting exon 16 of *celsr1a* were designed using Zifit (zifit.partners.org) (Sander et al., 2010). A mix of 150 ng/µl Cas9 mRNA, and 100 ng/µl gRNA was injected into *frnt*/+ one-cell stage embryos in a total volume of 2 nl. Fish were screened at young juvenile stages for appearance of the *frnt* phenotype.

Green fluorescent protein (GFP) was knocked-in 114 nucleotides upstream of the start codon of *celsr1a* using CRISPR/Cas9. One gRNA targeted close to the start codon was chosen based on CHOPCHOP prediction (http://chopchop.cbu.uib.no/)(Labun et al., 2019). A donor plasmid was constructed using 1 kb homology arms at each side of the insertion site. A mix of 125 ng/µl Cas9 mRNA (System Biosciences), 12.5 µM gRNA (IDT), 10 ng/µl donor plasmid and 1 mM SCR7 (Xcessbio Biosciences) was injected into wild-type one-cell stage embryos in a total volume of 2nl. Fish were screened at 24-72 hpf for the presence of GFP expression.

Histology

Fish were anesthetized by 0.4% MS-222 and fixed using 4% paraformaldehyde (PFA) at 4°C overnight, decalcified in 14% EDTA for one week before proceeding for dehydration and embedding in paraffin. Samples were cut at a 6 µm thickness and stained with Haematoxylin (Electron Miscroscopy Sciences) and Eosin (Sigma). For Alcian blue PAS staining, after deparaffinization and hydration to distilled water, slides were stained in 1% alcian blue solution (pH 2.5) for 30 min, then washed in running tap water for 2 min and rinsed in distilled water, then were oxidized in 0.5% periodic acid solution for 5 min, rinsed in distilled water and placed in Schiff's reagent for 15 min. For PAS stain, after *in situ hybridization* slides were oxidized in 0.5% periodic acid solution for 5 min, rinsed in distilled water and then placed in Schiff's reagent for 15 min for staining.

Muscle fibers were measured from individual sections stained with Hematoxalin and Eosin using Nikon NIS Elements software package v4.4 quantitation software. At least three individuals were counted from each genotype and age group, and fibers from both the left and right slow muscle were counted. Only one section was counted for each individual.

in situ hybridization

Probes for *in situ* hybridization were synthesized using DIG RNA Labeling Kit (Roche). *in situ* hybridization was carried out on paraffin sections. Slides were rehydrated, digested by proteinase K

and acetylated by treatment with acetic anhydride in triethanolamine. Sections were hybridized with approximately 10 ng probe in 100 µl hyb at 65∘C overnight. After post-hybridization wash and antibody incubation with anti-Digoxigenin-AP (1:2500 dilution), the signal was detected by BCIP/ NBT (Sigma).

For quantification of *olfm4* expression in intestines, we counted the average number of *olfm4* positive cells per section. Two to three sections per fish were counted; n=5-7 fish.

Electron microscopy

Excised samples of the flank encompassing slow muscle tissue of adult wild-type and *celsr1a* mutant fish were fixed with a mixture of 4% PFA in PBS and 1–2.5% glutaraldehyde. After post-fixation with 1% osmium tetroxide in 100mM PBS, samples were treated with 1% aqueous uranyl acetate, dehydrated through a graded series of ethanol and embedded in Epon. Ultrathin sections were stained with uranyl acetate and lead citrate and viewed in a Philips CM10 electron microscope housed at the Max Planck for Developmental Biology, Tübingen, Germany.

Southern Blot of telomere length

Genomic DNA was extracted by phenol-chloroform-isoamyl alcohol extraction method in order to obtain intact long telomeres, and was digested by HinfI, RsaI, AluI, MspI and HaeIII. 6 ug of total digested genomic DNA was loaded per lane. After electrophoresis, DNA was transferred to a positively charged nylon membrane. Probe labeling and Southern blot detection were carried out using 'DIG High Prime DNA Labeling and Detection Starter Kit I' (Roche). Probes were generated using PCR based amplification of the (TTAGGG) repeat only were used to amply fragment from telomere and subcoloned. Probe was labeled with digoxigenin-dUTP.

Western Blot

Tissue was isolated from 5 month old adult *frnt* mutant and wild-type fish and protein were extracted in RIPA buffer (Pierce ThermoScientific). 30 mg protein from tissues were loaded in 6% SDS-PAGE gel. Longer gel electrophoresis (150 V for 2.5 h) and transfer (15 V O/N) was conducted due to the predicted large size of Celsr1a protein. Western Blot was performed using 1:500 dilution of Celsr1a antibody (AnaSpec. Inc).

Skeletal staining and quantitation

Alizarin red staining was performed using 1% alizarin red in 0.5% KOH. Tissue was dehydrated in ethanol prior to staining. Measurement of scale diameter accomplished through quantitation tools within the Nikon NIS Elements software package v4.4.

SA-β-gal staining.

Fish tissues were fixed in 0.2% glutaraldehyde overnight, stained in 1mg/ml 5-Bromo-4-chloro-3-indolyl β-D-galactopyranoside (X-gal, Cell Signaling) pH of 5.9-6.1 overnight at 37C, and post-fixed in 4% PFA. The samples were then processed for paraffin embedding by standard dehydration methods. Cross-sections of these samples were cut at a 6 μm thickness and counterstained with nuclear red.

BrdU labeling.

For analysis of proliferation in larvae, 10 mM BrdU (Sigma) was added to E3 buffer and larvae were treated for 24h at 28.5°C. For analysis in adult tissues, 30 μl of 2.5 mg/mL BrdU (Sigma) was injected intraperitoneally and samples were collected at designated times after injection (Hui et al., 2014; Schall et al., 2017).

BrdU staining was conducted following (Verduzco and Amatruda, 2011) with minor modifications. In brief, larvae were fixed in 4%PFA for 2 h, then transferred to methanol at -20∘C. A 1:100 dilution was used for anti-BrdU antibody after 5 x 10 min wash in PBST. Adult tissues were dissected, fixed overnight, and processed for standard paraffin embedding. Cross-sections of these samples were cut at a 6 μm thickness and treated with standard immunofluorescence (1:500 dilution of BrdU antibody) with an antigen retrieval step of boiling in sodium citrate buffer (10 mM, pH 6) for 5 min. Slides were then counterstained with about 300 nM DAPI for 30 min.

Immunofluorescence.

Primary antibodies and dilutions: BrdU antibody (IIB5) (Santa Cruz Biotechnology sc-32323, 1:500), Phospho-Histone H3 (Ser10) (Cell Signaling Technology 9701, 1:500), Anti-GFP rabbit IgG, Alexa Fluor 555 conjugated (Invitrogen A-31851, 1:500), anti-GFP chicken IgY (Invitrogen A10262, 1:500). Secondary antibodies and dilutions: Alexa Fluor 488 goat anti-rabbit IgG (Invitrogen A11070, 1:500), Alexa Fluor 568 goat anti-rabbit IgG (H+L) (Invitrogen A21069, 1:500), Goat anti-mouse IgG (Cy3 (Abcam ab97035, 1:500), Alexa Fluor 488 goat anti-chicken IgG (Invitrogen A11039, 1:500). Before

blocking, sections were boiled in sodium citrate buffer (10mM, pH=6) for 5 min in a pressure cooker for antigen retrieval. Slides were then counterstained with about 300 nM DAPI for 30 min.

Caloric Restriction

Mutant or control fish were placed with an equal number of albino fish at normal rearing density (20/liter) per each feeding group tested. Albino fish were present to serve as a balance for fish density and buffer in the case of reduced viability in the study due to the mutant genotype. Two separate experiments were carried out, one with wildtype fish and the other with siblings as controls. Fish were sorted by phenotype at juvenile stages and placed on the experimental diets starting at 5 month and 3.5 months old, respectively. The caloric restriction feed was synthesized by reducing carbohydrate and proteins but maintaining the lipid and vitamins/mineral constant to avoid malnutrition. The ingredient and constitution of the feed is shown in **Suppl. Table 1**. To normalize feeding regimes, the amount of food was provided as a measure of total weight of the fish. Fish weight was measured *en masse* per group and not singularly every two weeks, and fish were fed at 3% of total fish weight. Fish numbers were counted weekly and any deaths were recorded daily. Experiments were terminated once the percentage of fish remaining dropped below 20% of starting numbers.

Statistical analysis

Values are shown as mean ± standard deviation. Statistical significance between two groups was determined by student's t-test. Statistical significance among several experimental groups was determined by one-way analysis of variance (ANOVA). Significance was set at $p<0.05$. Mantel-Cox and Geha-Brelow-Wilcoxon tests testing viability curves were executed using Prism software package.

REFERENCES

Adams, M. M. and Kafaligonul, H. (2018). Zebrafish-A Model Organism for Studying the Neurobiological Mechanisms Underlying Cognitive Brain Aging and Use of Potential Interventions. *Front Cell Dev Biol* **6**, 135.

Aghaallaei, N., Gruhl, F., Schaefer, C. Q., Wernet, T., Weinhardt, V., Centanin, L., Loosli, F., Baumbach, T. and Wittbrodt, J. (2016). Identification, visualization and clonal analysis of intestinal stem cells in fish. *Development* **143**, 3470-3480.

Allache, R., De Marco, P., Merello, E., Capra, V. and Kibar, Z. (2012). Role of the planar cell polarity gene CELSR1 in neural tube defects and caudal agenesis. *Birth Defects Res A Clin Mol Teratol* **94**, 176-181.

Altschul, S. F., Gish, W., Miller, W., Myers, E. W. and Lipman, D. J. (1990). Basic local alignment search tool. *J Mol Biol* **215**, 403-410.

Aman, A. J., Fulbright, A. N. and Parichy, D. M. (2018). Wnt/beta-catenin regulates an ancient signaling network during zebrafish scale development. *Elife* **7**.

An, Z., Sabalic, M., Bloomquist, R. F., Fowler, T. E., Streelman, T. and Sharpe, P. T. (2018). A quiescent cell population replenishes mesenchymal stem cells to drive accelerated growth in mouse incisors. *Nat Commun* **9**, 378.

Anchelin, M., Alcaraz-Perez, F., Martinez, C. M., Bernabe-Garcia, M., Mulero, V. and Cayuela, M. L. (2013). Premature aging in telomerase-deficient zebrafish. *Dis Model Mech* **6**, 1101-1112.

Arslan-Ergul, A., Erbaba, B., Karoglu, E. T., Halim, D. O. and Adams, M. M. (2016). Short-term dietary restriction in old zebrafish changes cell senescence mechanisms. *Neuroscience* **334**, 64-75.

Basak, O., Beumer, J., Wiebrands, K., Seno, H., van Oudenaarden, A. and Clevers, H. (2017). Induced Quiescence of Lgr5+ Stem Cells in Intestinal Organoids Enables Differentiation of Hormone-Producing Enteroendocrine Cells. *Cell Stem Cell* **20**, 177-190 e174.

Berberoglu, M. A., Gallagher, T. L., Morrow, Z. T., Talbot, J. C., Hromowyk, K. J., Tenente, I. M., Langenau, D. M. and Amacher, S. L. (2017). Satellite-like cells contribute to pax7-dependent skeletal muscle repair in adult zebrafish. *Dev Biol* **424**, 162-180.

Bishop, N. A. and Guarente, L. (2007). Genetic links between diet and lifespan: shared mechanisms from yeast to humans. *Nat Rev Genet* **8**, 835-844.

Blagosklonny, M. V. (2010). Calorie restriction: decelerating mTOR-driven aging from cells to organisms (including humans). *Cell Cycle* **9**, 683-688.

Bowen, M. E., Henke, K., Siegfried, K. R., Warman, M. L. and Harris, M. P. (2012). Efficient mapping and cloning of mutations in zebrafish by low-coverage whole-genome sequencing. *Genetics* **190**, 1017-1024.

Bronikowski, A. M. and Promislow, D. E. (2005). Testing evolutionary theories of aging in wild populations. *Trends Ecol Evol* **20**, 271-273.

Buczacki, S. J., Zecchini, H. I., Nicholson, A. M., Russell, R., Vermeulen, L., Kemp, R. and Winton, D. J. (2013). Intestinal label-retaining cells are secretory precursors expressing Lgr5. *Nature* **495**, 65-69.

Burtner, C. R. and Kennedy, B. K. (2010). Progeria syndromes and ageing: what is the connection? *Nat Rev Mol Cell Biol* **11**, 567-578.

Carneiro, M. C., de Castro, I. P. and Ferreira, M. G. (2016). Telomeres in aging and disease: lessons from zebrafish. *Dis Model Mech* **9**, 737-748.

Carreira-Barbosa, F., Kajita, M., Morel, V., Wada, H., Okamoto, H., Martinez Arias, A., Fujita, Y., Wilson, S. W. and Tada, M. (2009). Flamingo regulates epiboly and convergence/extension movements through cell cohesive and signalling functions during zebrafish gastrulation. *Development* **136**, 383-392.

Chen, H., Beasley, A., Hu, Y. and Chen, X. (2015). A Zebrafish Model for Studies on Esophageal Epithelial Biology. *PloS one* **10**, e0143878.

Chen, Z., Lei, Y., Cao, X., Zheng, Y., Wang, F., Bao, Y., Peng, R., Finnell, R. H., Zhang, T. and Wang, H. (2018). Genetic analysis of Wnt/PCP genes in neural tube defects. *BMC Med Genomics* **11**, 38.

Collado, M., Blasco, M. A. and Serrano, M. (2007). Cellular senescence in cancer and aging. *Cell* **130**, 223-233.

Cui, R., Medeiros, T., Willemsen, D., Iasi, L. N. M., Collier, G. E., Graef, M., Reichard, M. and Valenzano, D. R. (2019). Relaxed Selection Limits Lifespan by Increasing Mutation Load. *Cell* **178**, 385-399 e320.

Curtin, J. A., Quint, E., Tsipouri, V., Arkell, R. M., Cattanach, B., Copp, A. J., Henderson, D. J., Spurr, N., Stanier, P., Fisher, E. M., et al. (2003). Mutation of Celsr1 disrupts planar polarity of inner ear hair cells and causes severe neural tube defects in the mouse. *Curr Biol* **13**, 1129-1133.

Devenport, D. and Fuchs, E. (2008). Planar polarization in embryonic epidermis orchestrates global asymmetric morphogenesis of hair follicles. *Nat Cell Biol* **10**, 1257-1268.

Dimri, G. P., Lee, X., Basile, G., Acosta, M., Scott, G., Roskelley, C., Medrano, E. E., Linskens, M., Rubelj, I., Pereira-Smith, O., et al. (1995). A biomarker that identifies senescent human cells in culture and in aging skin in vivo. *Proc Natl Acad Sci U S A* **92**, 9363-9367.

Flasse, L. C., Stern, D. G., Pirson, J. L., Manfroid, I., Peers, B. and Voz, M. L. (2013). The bHLH transcription factor Ascl1a is essential for the specification of the intestinal secretory cells and mediates Notch signaling in the zebrafish intestine. *Dev Biol* **376**, 187-197.

Fontana, L. and Partridge, L. (2015). Promoting health and longevity through diet: from model organisms to humans. *Cell* **161**, 106-118.

Formstone, C. J. and Mason, I. (2005). Combinatorial activity of Flamingo proteins directs convergence and extension within the early zebrafish embryo via the planar cell polarity pathway. *Dev Biol* **282**, 320-335.

Fre, S., Huyghe, M., Mourikis, P., Robine, S., Louvard, D. and Artavanis-Tsakonas, S. (2005). Notch signals control the fate of immature progenitor cells in the intestine. *Nature* **435**, 964-968.

Genade, T., Benedetti, M., Terzibasi, E., Roncaglia, P., Valenzano, D. R., Cattaneo, A. and Cellerino, A. (2005). Annual fishes of the genus Nothobranchius as a model system for aging research. *Aging Cell* **4**, 223-233.

Goffinet, A. M. and Tissir, F. (2017). Seven pass Cadherins CELSR1-3. *Semin Cell Dev Biol* **69**, 102-110.

Guarente, L. (2013). Calorie restriction and sirtuins revisited. *Genes Dev* **27**, 2072-2085.

Guzman, A., Ramos-Balderas, J. L., Carrillo-Rosas, S. and Maldonado, E. (2013). A stem cell proliferation burst forms new layers of P63 expressing suprabasal cells during zebrafish postembryonic epidermal development. *Biol Open* **2**, 1179-1186.

Harel, I., Benayoun, B. A., Machado, B., Singh, P. P., Hu, C. K., Pech, M. F., Valenzano, D. R., Zhang, E., Sharp, S. C., Artandi, S. E., et al. (2015). A platform for rapid exploration of aging and diseases in a naturally short-lived vertebrate. *Cell* **160**, 1013-1026.

Harris, M. P., Rohner, N., Schwarz, H., Perathoner, S., Konstantinidis, P. and Nusslein-Volhard, C. (2008). Zebrafish eda and edar mutants reveal conserved and ancestral roles of ectodysplasin signaling in vertebrates. *PLoS Genet* **4**, e1000206.

Harty, B. L., Krishnan, A., Sanchez, N. E., Schioth, H. B. and Monk, K. R. (2015). Defining the gene repertoire and spatiotemporal expression profiles of adhesion G protein-coupled receptors in zebrafish. *BMC Genomics* **16**, 62.

Hatakeyama, H., Nakamura, K., Izumiyama-Shimomura, N., Ishii, A., Tsuchida, S., Takubo, K. and Ishikawa, N. (2008). The teleost Oryzias latipes shows telomere shortening with age despite considerable telomerase activity throughout life. *Mech Ageing Dev* **129**, 550-557.

Hatakeyama, H., Yamazaki, H., Nakamura, K., Izumiyama-Shimomura, N., Aida, J., Suzuki, H., Tsuchida, S., Matsuura, M., Takubo, K. and Ishikawa, N. (2016). Telomere attrition and restoration in the normal teleost Oryzias latipes are linked to growth rate and telomerase activity at each life stage. *Aging (Albany NY)* **8**, 62-76.

Henriques, C. M., Carneiro, M. C., Tenente, I. M., Jacinto, A. and Ferreira, M. G. (2013). Telomerase is required for zebrafish lifespan. *PLoS Genet* **9**, e1003214.

Hu, C. K. and Brunet, A. (2018). The African turquoise killifish: A research organism to study vertebrate aging and diapause. *Aging Cell* **17**, e12757.

Huang, X. and Madan, A. (1999). CAP3: A DNA sequence assembly program. *Genome Res* **9**, 868-877.

Hui, S. P., Sengupta, D., Lee, S. G., Sen, T., Kundu, S., Mathavan, S. and Ghosh, S. (2014). Genome wide expression profiling during spinal cord regeneration identifies comprehensive cellular responses in zebrafish. *PLoS One* **9**, e84212.

Igarashi, M. and Guarente, L. (2016). mTORC1 and SIRT1 Cooperate to Foster Expansion of Gut Adult Stem Cells during Calorie Restriction. *Cell* **166**, 436-450.

Jensen, J., Pedersen, E. E., Galante, P., Hald, J., Heller, R. S., Ishibashi, M., Kageyama, R., Guillemot, F., Serup, P. and Madsen, O. D. (2000). Control of endodermal endocrine development by Hes-1. *Nat Genet* **24**, 36-44.

Keller, E. T. and Murtha, J. M. (2004). The use of mature zebrafish (Danio rerio) as a model for human aging and disease. *Comp Biochem Physiol C Toxicol Pharmacol* **138**, 335-341.

Kenyon, C. J. (2010). The genetics of ageing. *Nature* **464**, 504-512.

Keyes, W. M., Wu, Y., Vogel, H., Guo, X., Lowe, S. W. and Mills, A. A. (2005). p63 deficiency activates a program of cellular senescence and leads to accelerated aging. *Genes Dev* **19**, 1986-1999.

Kim, D. H., Park, M. H., Lee, E. K., Choi, Y. J., Chung, K. W., Moon, K. M., Kim, M. J., An, H. J., Park, J. W., Kim, N. D., et al. (2015). The roles of FoxOs in modulation of aging by calorie restriction. *Biogerontology* **16**, 1-14.

Kirschner, J., Weber, D., Neuschl, C., Franke, A., Bottger, M., Zielke, L., Powalsky, E., Groth, M., Shagin, D., Petzold, A., et al. (2012). Mapping of quantitative trait loci controlling lifespan in the short-lived fish Nothobranchius furzeri--a new vertebrate model for age research. *Aging Cell* **11**, 252-261.

Kishi, S., Bayliss, P. E., Uchiyama, J., Koshimizu, E., Qi, J., Nanjappa, P., Imamura, S., Islam, A., Neuberg, D., Amsterdam, A., et al. (2008). The identification of zebrafish mutants showing alterations in senescence-associated biomarkers. *PLoS Genet* **4**, e1000152.

Kokubu, H., Ohtsuka, T. and Kageyama, R. (2008). Mash1 is required for neuroendocrine cell development in the glandular stomach. *Genes Cells* **13**, 41-51.

Koshimizu, E., Imamura, S., Qi, J., Toure, J., Valdez, D. M., Jr., Carr, C. E., Hanai, J. and Kishi, S. (2011). Embryonic senescence and laminopathies in a progeroid zebrafish model. *PLoS One* **6**, e17688.

Kuzmichev, A. N., Kim, S. K., D'Alessio, A. C., Chenoweth, J. G., Wittko, I. M., Campanati, L. and McKay, R. D. (2012). Sox2 acts through Sox21 to regulate transcription in pluripotent and differentiated cells. *Current biology : CB* **22**, 1705-1710.

Labun, K., Montague, T. G., Krause, M., Torres Cleuren, Y. N., Tjeldnes, H. and Valen, E. (2019). CHOPCHOP v3: expanding the CRISPR web toolbox beyond genome editing. *Nucleic Acids Res*.

Le Garrec, J. F. and Kerszberg, M. (2008). Modeling polarity buildup and cell fate decision in the fly eye: insight into the connection between the PCP and Notch pathways. *Dev Genes Evol* **218**, 413-426.

Lee, B. Y., Han, J. A., Im, J. S., Morrone, A., Johung, K., Goodwin, E. C., Kleijer, W. J., DiMaio, D. and Hwang, E. S. (2006). Senescence-associated beta-galactosidase is lysosomal beta-galactosidase. *Aging Cell* **5**, 187-195.

Li, H. J., Ray, S. K., Singh, N. K., Johnston, B. and Leiter, A. B. (2011). Basic helix-loop-helix transcription factors and enteroendocrine cell differentiation. *Diabetes Obes Metab* **13 Suppl 1**, 5-12.

Lickwar, C. R., Camp, J. G., Weiser, M., Cocchiaro, J. L., Kingsley, D. M., Furey, T. S., Sheikh, S. Z. and Rawls, J. F. (2017). Genomic dissection of conserved transcriptional regulation in intestinal epithelial cells. *PLoS Biol* **15**, e2002054.

Liu, L. and Rando, T. A. (2011). Manifestations and mechanisms of stem cell aging. *J Cell Biol* **193**, 257-266.

Mouchiroud, L., Houtkooper, R. H., Moullan, N., Katsyuba, E., Ryu, D., Canto, C., Mottis, A., Jo, Y. S., Viswanathan, M., Schoonjans, K., et al. (2013). The NAD(+)/Sirtuin Pathway Modulates Longevity through Activation of Mitochondrial UPR and FOXO Signaling. *Cell* **154**, 430-441.

Murdoch, J. N., Damrau, C., Paudyal, A., Bogani, D., Wells, S., Greene, N. D., Stanier, P. and Copp, A. J. (2014). Genetic interactions between planar cell polarity genes cause diverse neural tube defects in mice. *Dis Model Mech* **7**, 1153-1163.

Novak, C. M., Jiang, X., Wang, C., Teske, J. A., Kotz, C. M. and Levine, J. A. (2005). Caloric restriction and physical activity in zebrafish (Danio rerio). *Neurosci Lett* **383**, 99-104.

Papan, C. and Campos-Ortega, J. A. (1994). On the formation of the neural keel and neural tube in the zebrafishDanio (Brachydanio) rerio. *Roux Arch Dev Biol* **203**, 178-186.

Pellegrinet, L., Rodilla, V., Liu, Z., Chen, S., Koch, U., Espinosa, L., Kaestner, K. H., Kopan, R., Lewis, J. and Radtke, F. (2011). Dll1- and dll4-mediated notch signaling are required for homeostasis of intestinal stem cells. *Gastroenterology* **140**, 1230-1240 e1231-1237.

Que, J., Okubo, T., Goldenring, J. R., Nam, K. T., Kurotani, R., Morrisey, E. E., Taranova, O., Pevny, L. H. and Hogan, B. L. (2007). Multiple dose-dependent roles for Sox2 in the patterning and differentiation of anterior foregut endoderm. *Development* **134**, 2521-2531.

Ravni, A., Qu, Y., Goffinet, A. M. and Tissir, F. (2009). Planar cell polarity cadherin Celsr1 regulates skin hair patterning in the mouse. *J Invest Dermatol* **129**, 2507-2509.

Reznick, D., Bryant, M. and Holmes, D. (2006). The evolution of senescence and post-reproductive lifespan in guppies (Poecilia reticulata). *PLoS Biol* **4**, e7.

Reznick, D. N., Bryant, M. J., Roff, D., Ghalambor, C. K. and Ghalambor, D. E. (2004). Effect of extrinsic mortality on the evolution of senescence in guppies. *Nature* **431**, 1095-1099.

Riccio, O., van Gijn, M. E., Bezdek, A. C., Pellegrinet, L., van Es, J. H., Zimber-Strobl, U., Strobl, L. J., Honjo, T., Clevers, H. and Radtke, F. (2008). Loss of intestinal crypt progenitor cells owing to inactivation of both Notch1 and Notch2 is accompanied by derepression of CDK inhibitors p27Kip1 and p57Kip2. *EMBO Rep* **9**, 377-383.

Robinson, A., Escuin, S., Doudney, K., Vekemans, M., Stevenson, R. E., Greene, N. D., Copp, A. J. and Stanier, P. (2012). Mutations in the planar cell polarity genes CELSR1 and SCRIB are associated with the severe neural tube defect craniorachischisis. *Hum Mutat* **33**, 440-447.

Robison, B. D., Drew, R. E., Murdoch, G. K., Powell, M., Rodnick, K. J., Settles, M., Stone, D., Churchill, E., Hill, R. A., Papasani, M. R., et al. (2008). Sexual dimorphism in hepatic gene expression and the response to dietary carbohydrate manipulation in the zebrafish (Danio rerio). *Comp Biochem Physiol Part D Genomics Proteomics* **3**, 141-154.

Rohner, N., Perathoner, S., Frohnhofer, H. G. and Harris, M. P. (2011). Enhancing the efficiency of N-ethyl-N-nitrosourea-induced mutagenesis in the zebrafish. *Zebrafish* **8**, 119-123.

Sander, J. D., Maeder, M. L., Reyon, D., Voytas, D. F., Joung, J. K. and Dobbs, D. (2010). ZiFiT (Zinc Finger Targeter): an updated zinc finger engineering tool. *Nucleic Acids Res* **38**, W462-468.

Schall, K. A., Holoyda, K. A., Isani, M., Schlieve, C., Salisbury, T., Khuu, T., Debelius, J. W., Moats, R. A., Pollack, H. A., Lien, C. L., et al. (2017). Intestinal adaptation in proximal and distal segments: Two epithelial responses diverge after intestinal separation. *Surgery* **161**, 1016-1027.

Schultz, M. B. and Sinclair, D. A. (2016). When stem cells grow old: phenotypes and mechanisms of stem cell aging. *Development* **143**, 3-14.

Seale, P., Sabourin, L. A., Girgis-Gabardo, A., Mansouri, A., Gruss, P. and Rudnicki, M. A. (2000). Pax7 is required for the specification of myogenic satellite cells. *Cell* **102**, 777-786.

Sei, Y., Feng, J., Samsel, L., White, A., Zhao, X., Yun, S., Citrin, D., McCoy, J. P., Sundaresan, S., Hayes, M. M., et al. (2018). Mature enteroendocrine cells contribute to basal and pathological stem cell dynamics in the small intestine. *Am J Physiol Gastrointest Liver Physiol* **315**, G495-G510.

Shi, D., Komatsu, K., Hirao, M., Toyooka, Y., Koyama, H., Tissir, F., Goffinet, A. M., Uemura, T. and Fujimori, T. (2014). Celsr1 is required for the generation of polarity at multiple levels of the mouse oviduct. *Development* **141**, 4558-4568.

Speakman, J. R. and Mitchell, S. E. (2011). Caloric restriction. *Mol Aspects Med* **32**, 159-221.

Sugimura, R., He, X. C., Venkatraman, A., Arai, F., Box, A., Semerad, C., Haug, J. S., Peng, L., Zhong, X. B., Suda, T., et al. (2012). Noncanonical Wnt signaling maintains hematopoietic stem cells in the niche. *Cell* **150**, 351-365.

Terzibasi, E., Valenzano, D. R. and Cellerino, A. (2007). The short-lived fish Nothobranchius furzeri as a new model system for aging studies. *Exp Gerontol* **42**, 81-89.

Tissir, F. and Goffinet, A. M. (2013). Atypical cadherins Celsr1-3 and planar cell polarity in vertebrates. *Prog Mol Biol Transl Sci* **116**, 193-214.

Valenzano, D. R., Sharp, S. and Brunet, A. (2011). Transposon-Mediated Transgenesis in the Short-Lived African Killifish Nothobranchius furzeri, a Vertebrate Model for Aging. *G3 (Bethesda)* **1**, 531-538.

van der Flier, L. G., Haegebarth, A., Stange, D. E., van de Wetering, M. and Clevers, H. (2009). OLFM4 is a robust marker for stem cells in human intestine and marks a subset of colorectal cancer cells. *Gastroenterology* **137**, 15-17.

van Es, J. H., van Gijn, M. E., Riccio, O., van den Born, M., Vooijs, M., Begthel, H., Cozijnsen, M., Robine, S., Winton, D. J., Radtke, F., et al. (2005). Notch/gamma-secretase inhibition turns proliferative cells in intestinal crypts and adenomas into goblet cells. *Nature* **435**, 959-963.

Verduzco, D. and Amatruda, J. F. (2011). Analysis of cell proliferation, senescence, and cell death in zebrafish embryos. *Methods Cell Biol* **101**, 19-38.

Vijg, J. and Suh, Y. (2005). Genetics of longevity and aging. *Annu Rev Med* **56**, 193-212.

Wallace, K. N., Akhter, S., Smith, E. M., Lorent, K. and Pack, M. (2005). Intestinal growth and differentiation in zebrafish. *Mech Dev* **122**, 157-173.

Wang, L., Xiao, Y., Tian, T., Jin, L., Lei, Y., Finnell, R. H. and Ren, A. (2018). Digenic variants of planar cell polarity genes in human neural tube defect patients. *Mol Genet Metab* **124**, 94-100.

Wang, Y., Williams, J., Rattner, A., Wu, S., Bassuk, A. G., Goffinet, A. M. and Nathans, J. (2016). Patterning of papillae on the mouse tongue: A system for the quantitative assessment of planar cell polarity signaling. *Dev Biol* **419**, 298-310.

Zhao, X. and Pack, M. (2017). Modeling intestinal disorders using zebrafish. *Methods Cell Biol* **138**, 241-270.

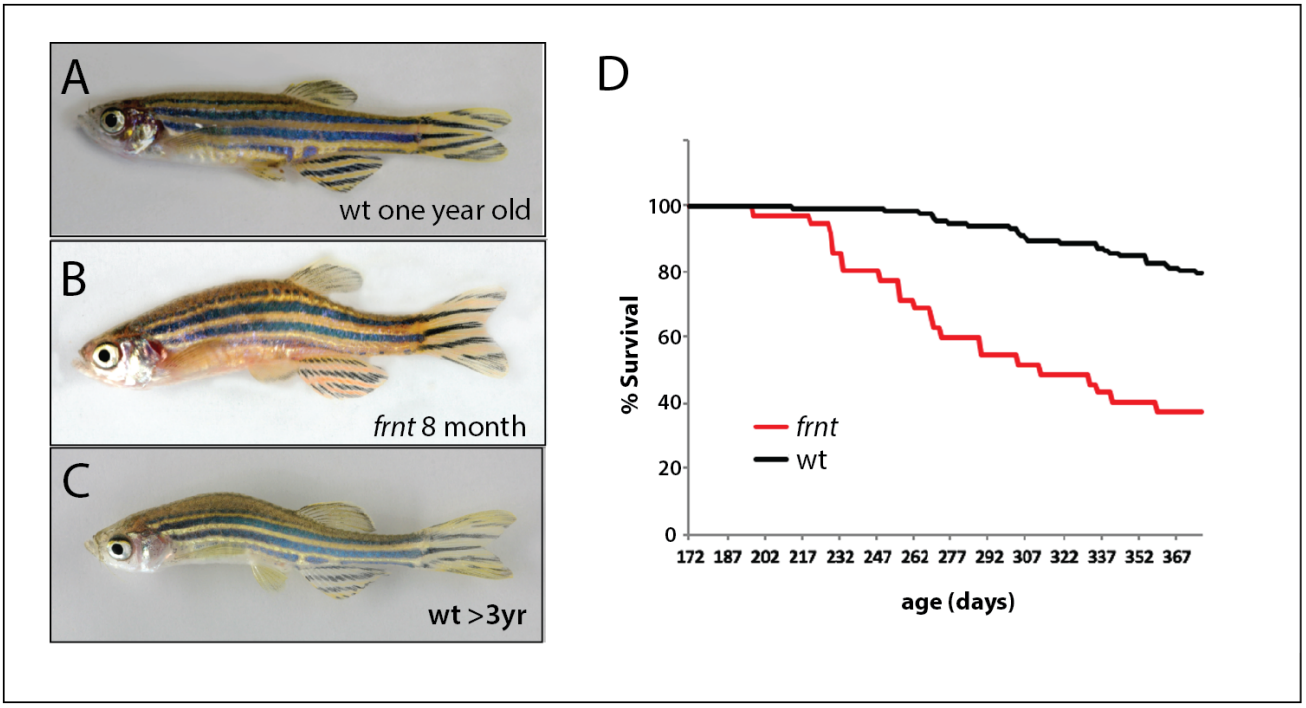

Figure 1. Identification of a zebrafish mutant, *fruehrentner (frnt)*, exhibiting late phenotypes that resemble normal aging. **A-C**) Aging phenotypes of young *frnt* mutant and old wild-type (wt) zebrafish. **B**) Appearance of adult *frnt* mutant showing ruffled appearance and kyphosis at young adult stages closely resembles that of old fish (**C**) compared to a (**A**) wild-type fish of similar age. **D**) *frnt* shows progressive loss of survival compared with wild-type fish.

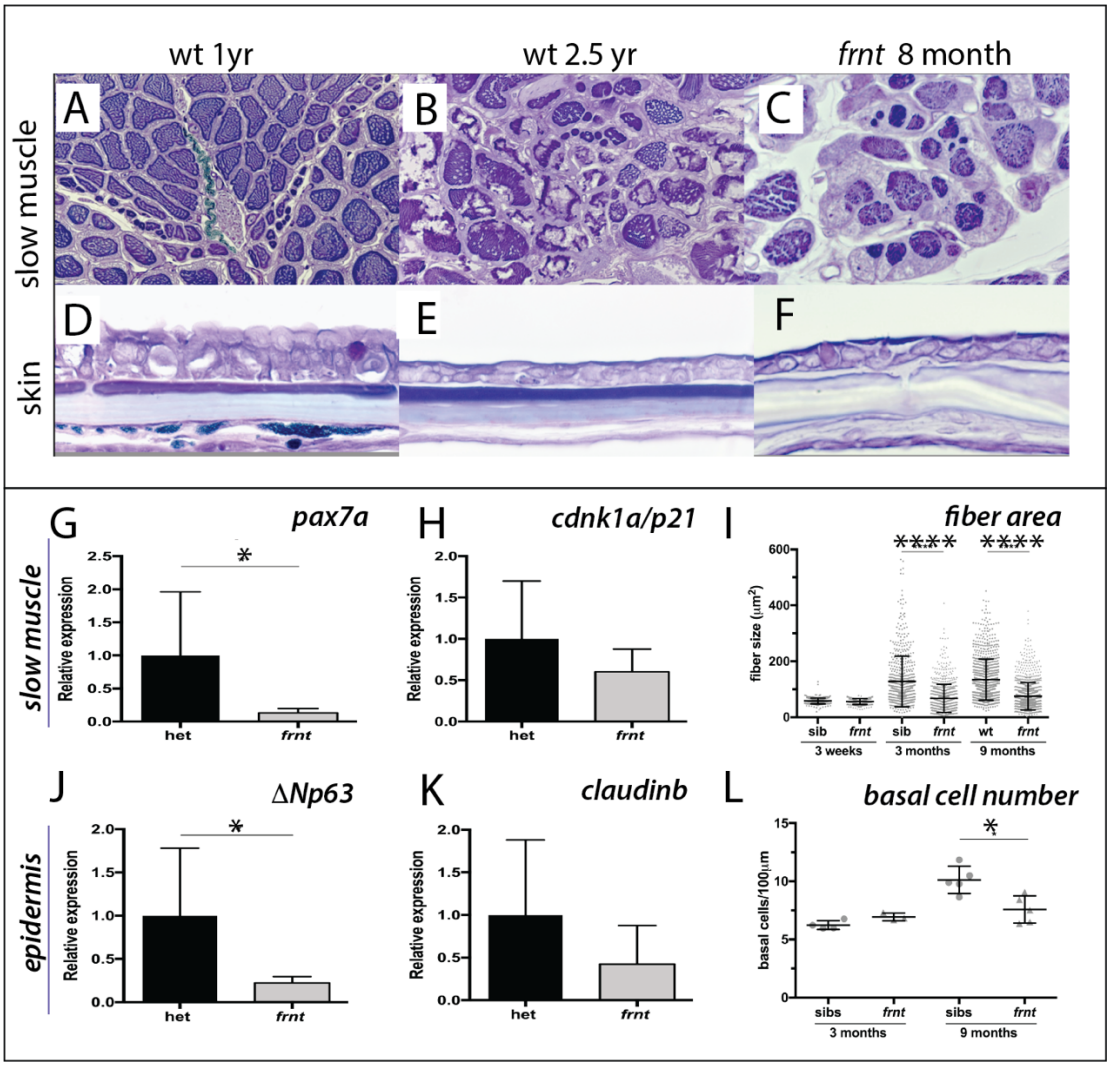

Figure 2. *frnt* causes acquired deficiencies resembling normal aging. A-F) Direct comparison of *frnt* with young adult, (**A, D**) and naturally aging wild-type zebrafish (2.5 years; **B, E**). Similar degenerative pathologies are shared between aged zebrafish (**B, E**) and 8 month-old mutants (**C, F**), such as fibrosis and sarcopenia of slow muscle fibers (**B, C**), and thinning skin (**E, F**). **G-I**) Characterization of slow muscle phenotype in *frnt* mutants. **G**) Expression analysis of stem cell marker *paired-box 7a* (*pax7a*) and (**H**) *cdnk1a*/*p21* control in slow muscle from 7 month old homozygous and heterozygous mutant fish. **I**) Adult *frnt* has smaller fiber size in slow muscle compared to age-matched wt and siblings (3 and 9 months old), but not as juvenile fish (3 week old). **J-L**) Changes in epidermal phenotype in *frnt* mutants. **J, K**) Expression of the stem cell marker *delta-Np63* and (**L**) control *claudinb* in epidermal tissues from 7 month old homozygous and heterozygous *frnt* fish. **L)** Count of DAPI positive basal cells in the integumentary epithelium in 3 and 9 month old fish. Error represented as mean +/- standard deviation. **** $p<0.0001$, * $p<0.05$.

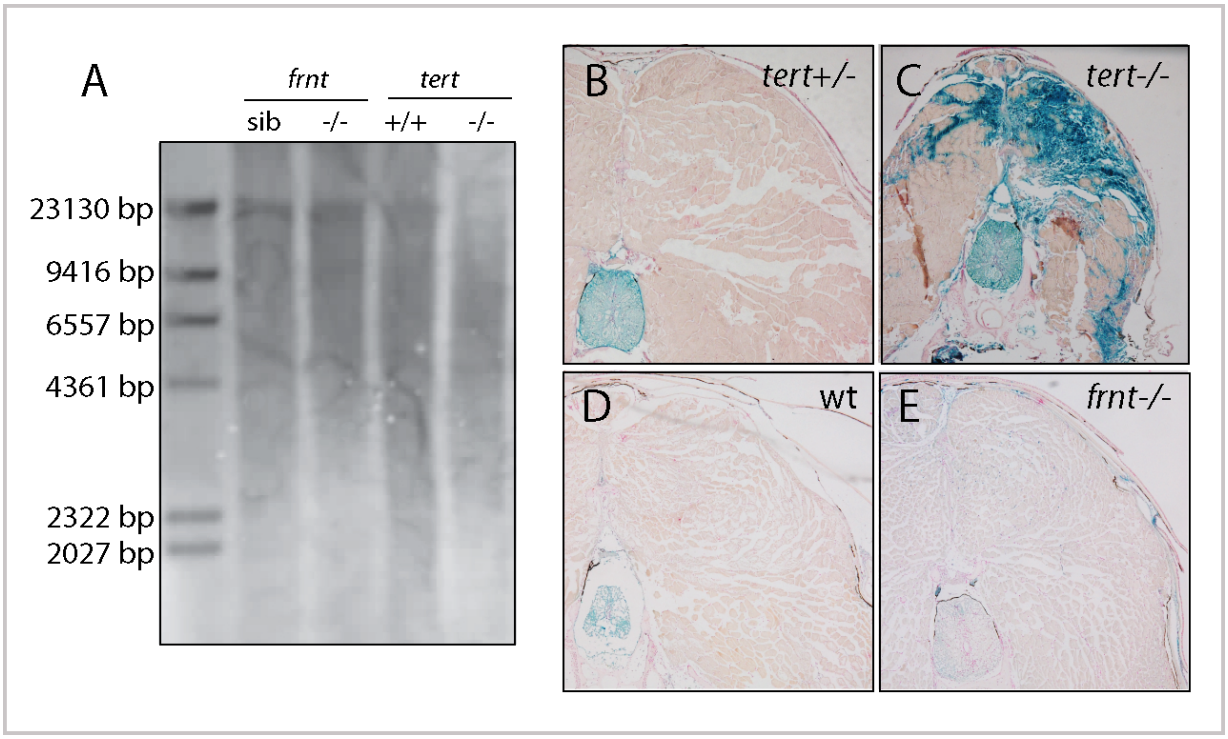

Figure 3. *frnt* mutation does not affect senescence biomarkers. A) Southern blot of genomic DNA of zebrafish *telomerase reverse transcriptase* (*tert*) and *frnt* mutants probed for telomere repeats. Data shows no effect of the mutation on telomere length in the *frnt* mutant compared with significant decrease of intensity and size of telomere in *tert* deficient fish. **B-E**). Senescence-associated beta-galactosidase (SA-βgal) staining (blue) of *frnt* mutants (E) and wild-type are matched fish (D) showed no significant difference, while *tert* mutants of comparable age showed a strong increase in staining (B, C). Samples were counterstained with nuclear red.

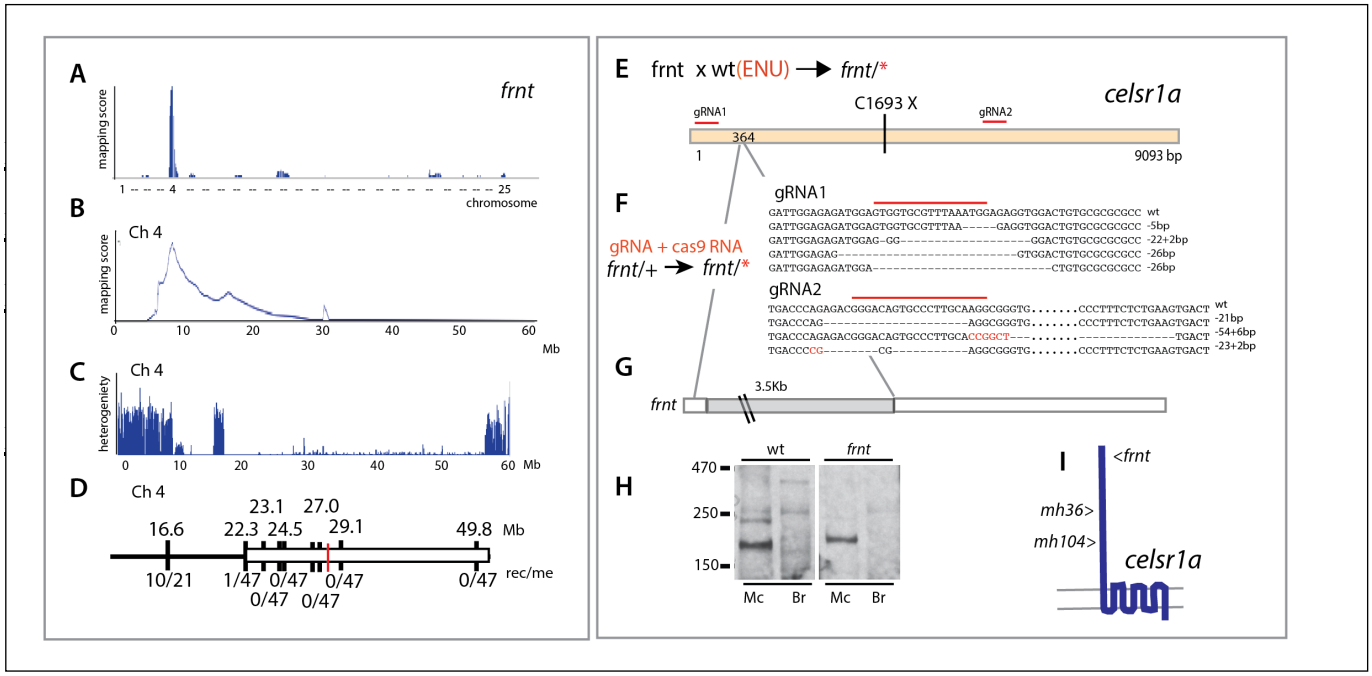

Figure 4. Identification of altered *celsr1a* function underlying the *frnt* phenotype. A). Mapping by homozygosity-by-descent indicates linkage of *frnt* to chromosome 4. **B**) Mapping score across chromosome 4. **C**) Analysis of heterogeneity across chromosome 4 showing a broad region of homogeneity in the population indicating linkage. **D**) Fine mapping of *frnt* showing limited recombination and resolution of the map position along chromosome 4; *white bar*, area showing linkage; red hashmark, position of *celsr1a*; top, position (megabase, Mb) on chromosome 4, zv9 assembly (https://ensembl.org); bottom number of recombinants per meiosis (rec/me) scored. **E**) Chemical mutagenesis loss-of-complementation screen to identify the gene mutation underlying the *frnt* phenotype. Exome sequencing of identified founders having the *frnt* phenotype (*frnt*/*), identified mutations in the *celsr1a* gene within the mapped interval (*mh36,* C1693X). **F**) Identified deletions/insertions within *celsr1a* generated through CRISPR/Cas9 genome editing that fail to complement *frnt*. Recovered sequences from F1 founders; guideRNA position demarcated with overlain red bar. Of the recovered lines, allele *mh104/P2027A-fs11X* was retained **G**) Identification of transposon insertion within *celsr1a* in *frnt.* **H**) Western analysis of *frnt* mutants show reduction of protein expression in the mutants; *Mc*, adult muscle; *Br*, adult brain. **I)** Schematic of *celsr1a* and position of identified mutations.

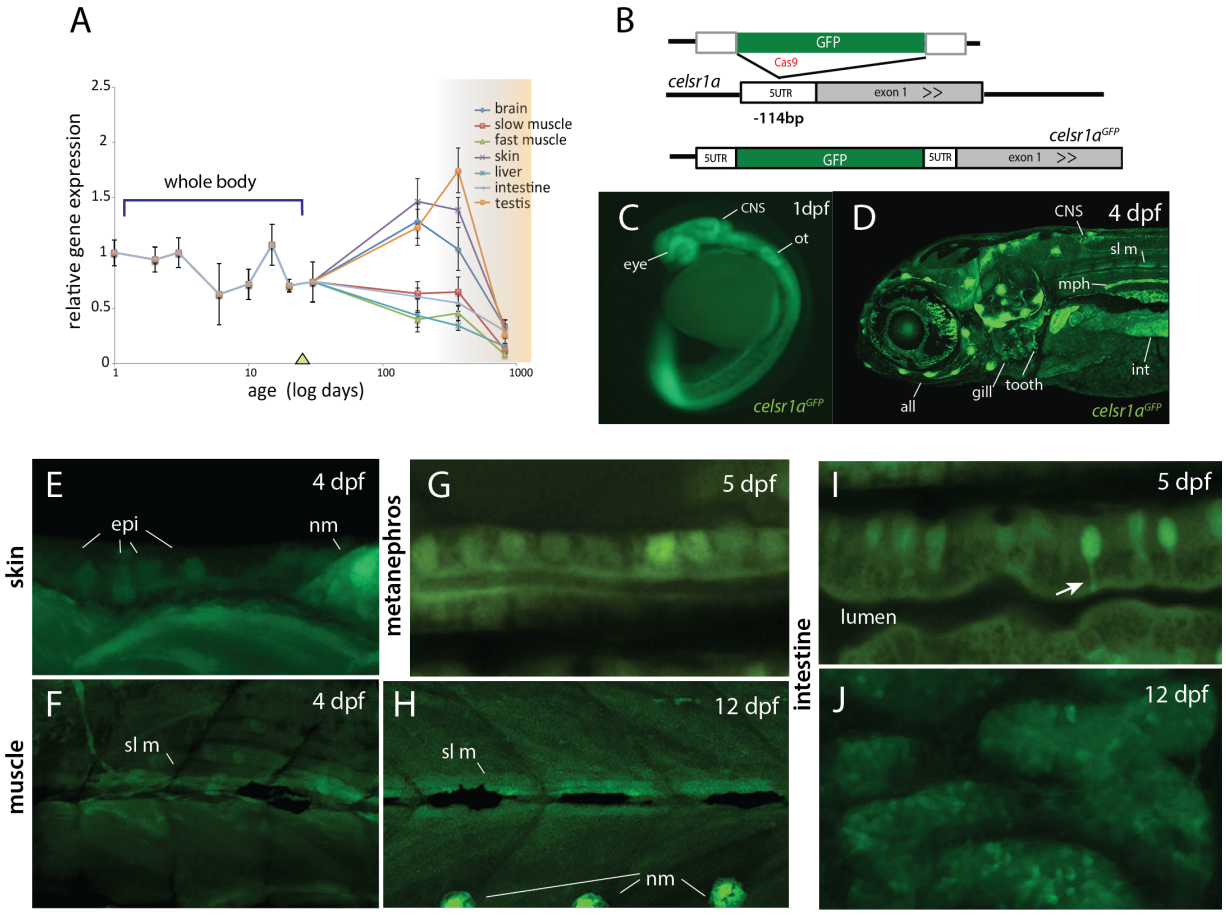

Figure 5. ***celsr1a*** **expression during development and as a function of age in adults. A**) qRT-PCR of *celsr1a* expression in larvae, juvenile, and adult stages showing a specific decrease in older fish concomitant with onset of senescent phenotypes and heightened age (ochre). During first 30 days of growth, expression in the whole body was assessed. After maturation (triangle on x axis), select tissues were assessed for changes in *celsr1a* expression. Data presented as mean +/-standard deviation. **B)** Strategy for GFP insertion at the *celsr1a* endogenous locus by homology directed repair. **C)** Expression of GFP in isolated *celsr1a*$^{GFP/+}$ transgenic line showing early expression of *celsr1a* in central nervous system (CNS), peripheral nervous system (PNS), and gut. **D-J)** Expression of *celsr1a*$^{GFP/+}$ transgene in larval and juvenile zebrafish showing progressive restriction and localization to specific cell types and tissues. *all*, anterior lateral line; *epi*, epidermal cells; *int*, intestine; *mph*, metanephros; *nm*, neuromast; *sl m*, slow muscle; *ot*, otolith.

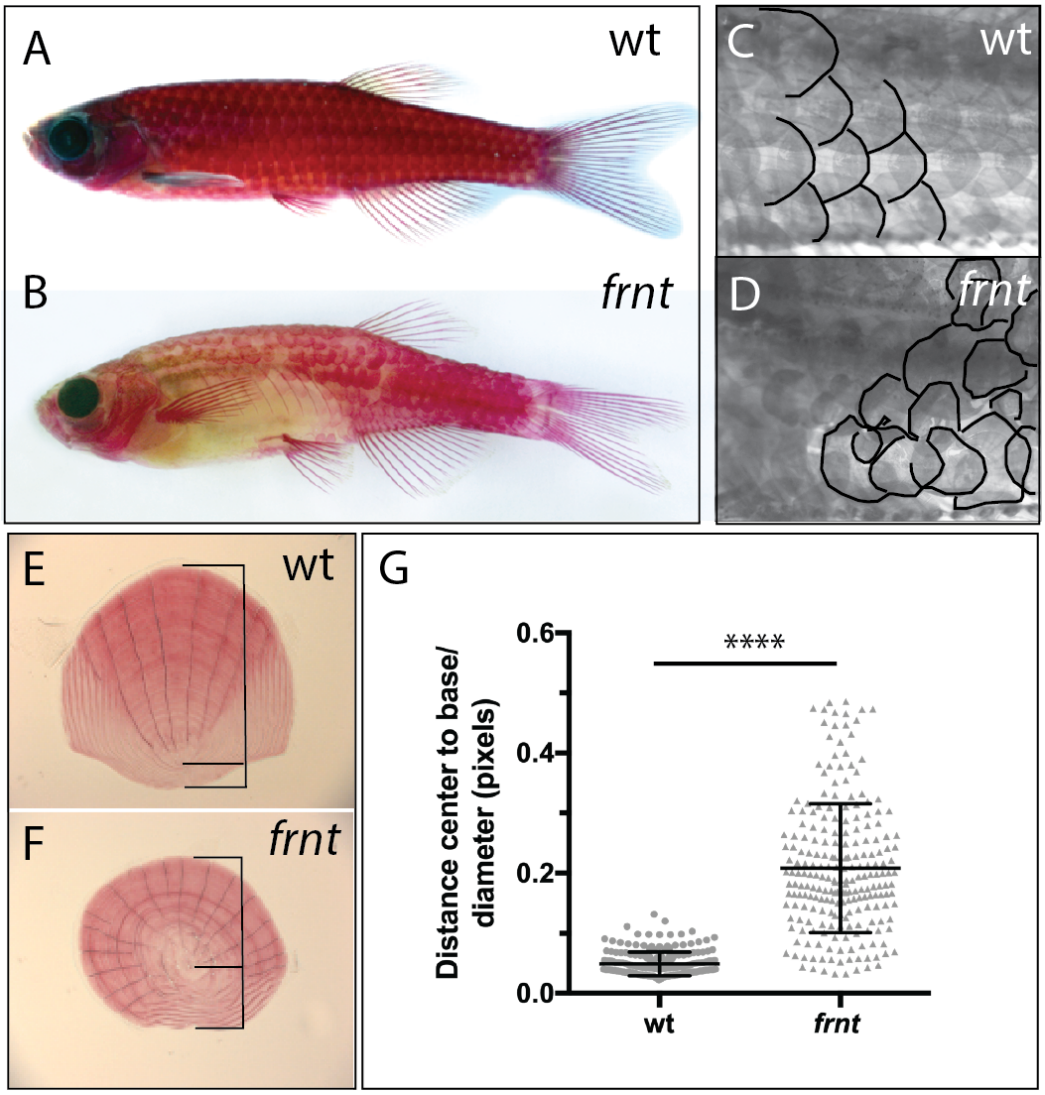

Figure 6. Loss of *celsr1a* leads to altered polarity phenotypes in the zebrafish integument. A) Alizarin red stained young adult wild-type zebrafish showing normal, regularly spaced pattern of scales across the flank. **C**) Close up of pattern in wild-type (wt) siblings, outline details posterior margin of scale. **B)**. Juvenile *frnt* mutant (10-12 week old) showing altered maturation of scales across the flank. **D**) Adult *frnt* showing 'whirling' pattern of scales. **E**) Wild-type scale showing internal polarity of growth along the rostrocaudal axis (bottom to top). **F**) *frnt* scale showing spiraling pattern, losing the internal polarity. **G**) Quantification of wild-type sibling and *frnt* scale polarity as indicated by the ratio of the center-to-base normalized by the diameter for each scale (**E, F**). Data presented as mean ± standard deviation; **** $p<0.001$.

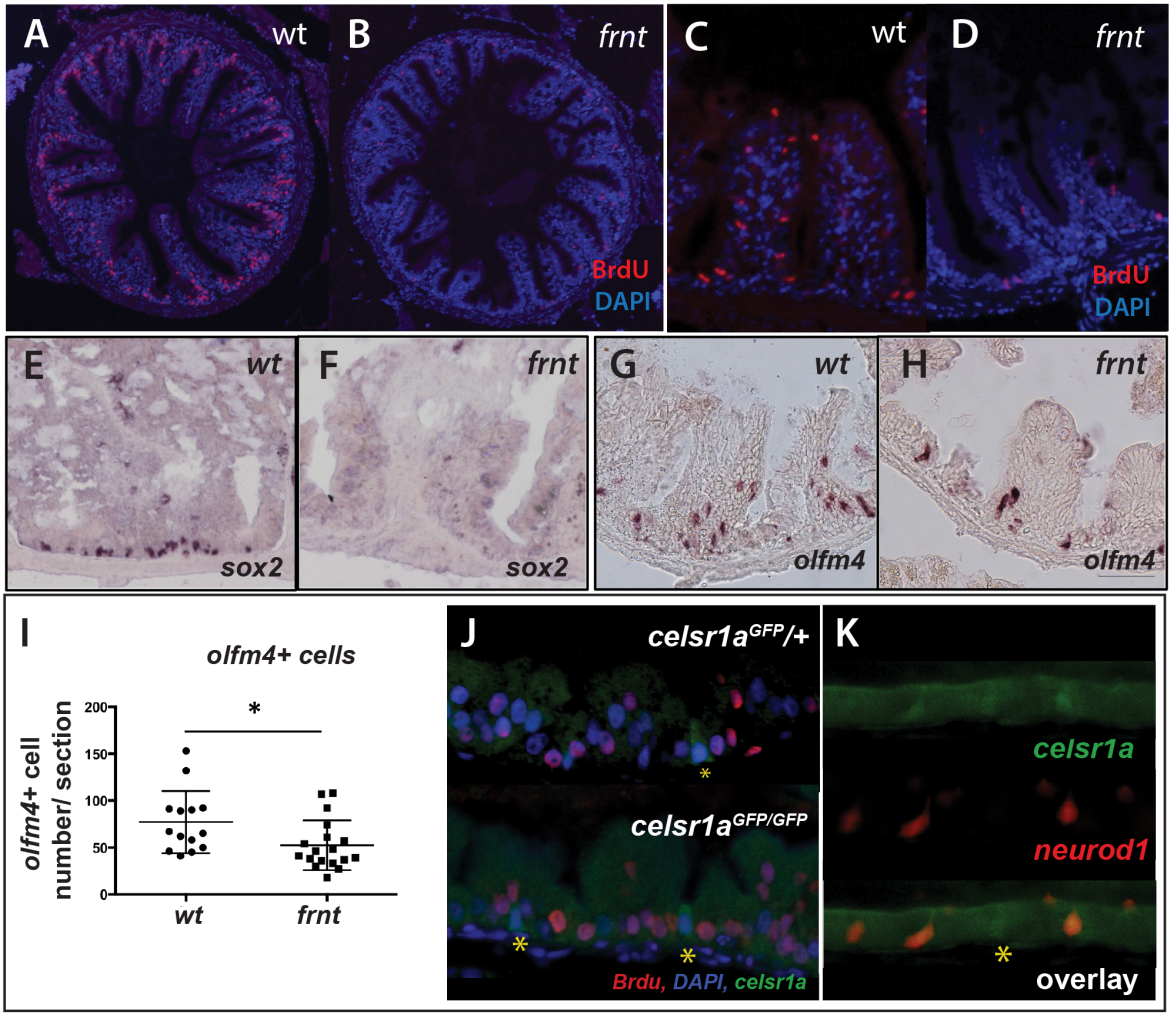

Figure 7. ***celsr1a*** **is essential for activity and maintenance of progenitor cells. A-D)** Analysis of proliferative capacity of the adult intestine in *celsr1a* mutants and age matched wild-type fish (pulse injection and incorporation after 4 hrs (red), nuclei counterstained by DAPI. **A, B)** Low power view of comparable posterior regions of intestine of wild-type (**A**) and age and size matched *frnt* mutants (**B**). **C, D)** Close up of intestinal rugae showing cells incorporating BrdU. **E-H)**, *in situ* hybridization of expression of *sex-determining region Y-box 2* (*sox2*) (**E, F**) and *olfactomedin 4* (*olfm4*). (**G, H**) genese in adult intestinal epithelia of wild-type (**E, G**) and *celsr1a* mutant (**F, H**) zebrafish. **I)** Quantitation of changes in the number of *olfm4*$^{+}$ cells observed in mutants; data presented as mean +/- standard deviation, * $p<0.05$, n=5 (wt sibling), n=7 (*frnt*) **J**) Proliferative cells (24hr after BrdU pulse, red) in comparison to *celsr1a* expression (*green*, yellow asterisk) in larval developing intestine at 4 dpf; DAPI, blue. **K)** co-expression of *celsr1a* (*celsr1a*$^{GFP/+}$) and *neurod1* (*Tg(neurod1:TagRFP)*) in 4 dpf intestine; asterisk highights *celsr1a*$^{+}$ without *neurod1* expression; all pictures luminal side placed on top.

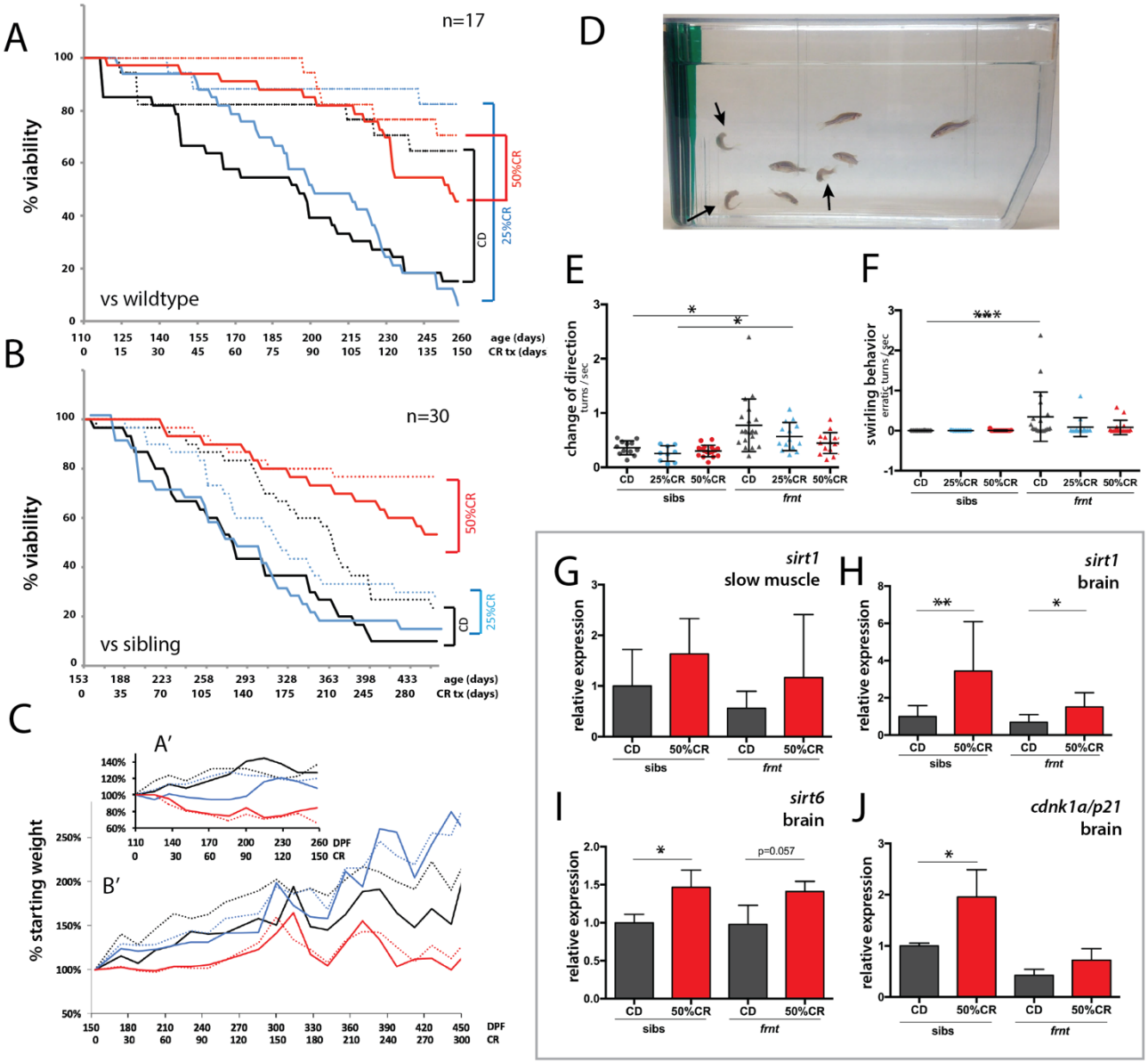

Figure 8. Caloric restriction increases longevity and alleviates pathology of *celsr1a/frnt* mutants. **A-C**) Effects of specialized diets, having no restriction (control diet (CD), black), 25% (blue) or 50% (red) calorie restriction (CR), on viability of zebrafish; *solid line*, *frnt* mutant; *dotted line*, control fish. **A-B**) Effect of specific reduction in calories on longevity; 50% caloric reduction lead to significant reduction in lethality of mutant and siblings compared to control and 25% caloric restricted diets; 50% CR diets for both mutant and sliblings are all $p<0.001$ compared to control and 25%CR diets by Mantel-Cox and Geha-Brelow-Wilcoxon tests. **C)** Analysis of average weight gain per treatment group for both experiments (A' and B'). **D-F)** Caloric restriction ameliorates aberrant swimming

behavior in *celsr1a* mutants. **D)** High frequency turning behavior of mutants in tank (arrows). Quantitation of change in direction (**E**) and erratic turns (**F**) in treatment groups with different levels of caloric reduction. **G-J**) Expression of genes associated with senescence and lifespan: **G, H)** *sirt1* (**G** - slow muscle and **H** - brain); **I)** *sirt6* (brain) and **J)** *cdnk1a*/*p21* (brain); data represented as mean ± standard deviation.

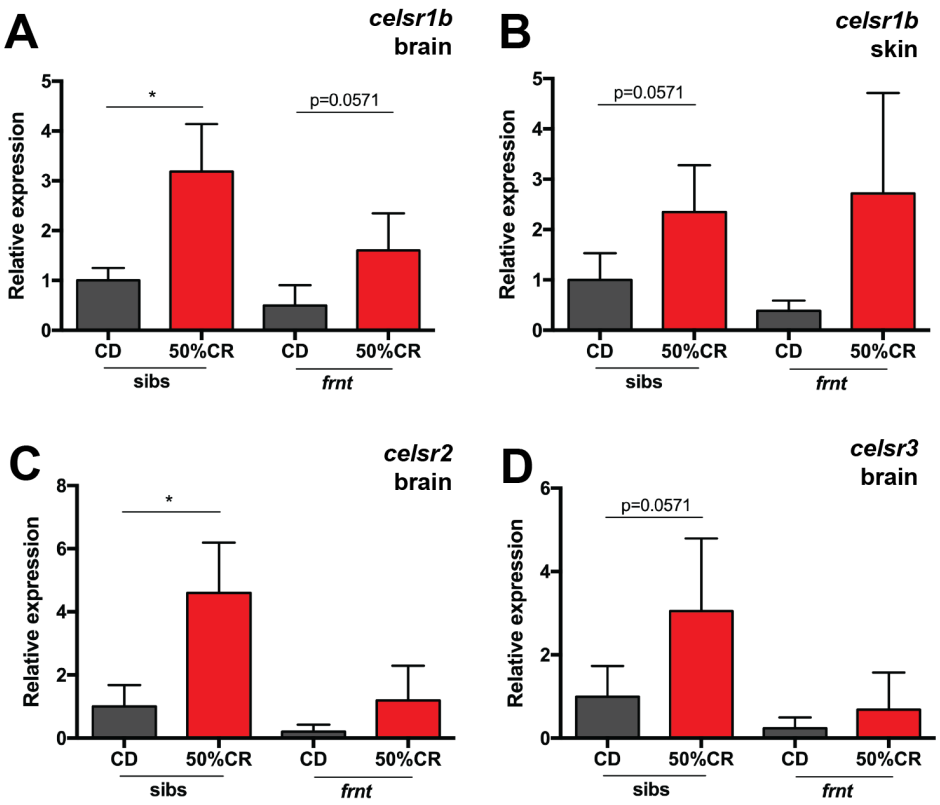

Figure 9. Compensatory responses of celsr1 homologues to caloric restriction. qRT-PCR analysis of *celsr1* homologues in *frnt* and wild-type sibling fish raised on normal and restricted diet (50% calorie restriction). Samples derived from 9 month old fish at end of treatment (after 5 month diet; n=4 per genotype). **A-B)** Expression of *celsr1b* paralogue in brain (**A**) and skin tissue (**B**). **C-D**) Expression of orthologues *celsr2* (**C**) and *celsr3* (**D**) in brain tissue. *p<0.05; data represented as mean +/- standard deviation.

SUPPLEMENTARY FIGURES

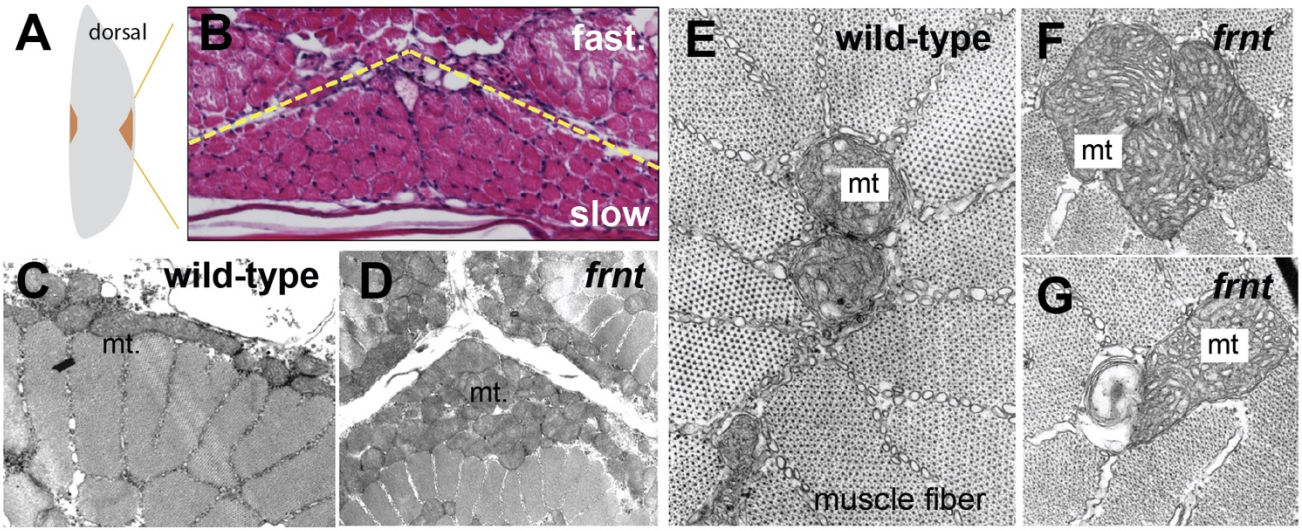

Supplementary Figure 1. ***Celsr1a*** **affects mitochondrial proliferation and maintenance. A)** Schematic of hemisected zebrafish flank with position of midline slow muscle populations outlined. **B**) Histological section of flank of a mature zebrafish showing organization of individual muscle fibers at the midline; Haematoxylin-eosin stain; yellow dotted line indicates boundary between slow and fast muscles. **C-G**) Transmission electron micrographs of slow muscle fibers showing medial and peripheral mitochondria (mt) from wild-type (**C,E**) and *frnt* mutant (**D**,**F,G**). *frnt* mutants show mitochondrial phenotypes of hyperproliferation (**D, F**), and evidence of degeneration (**G**).

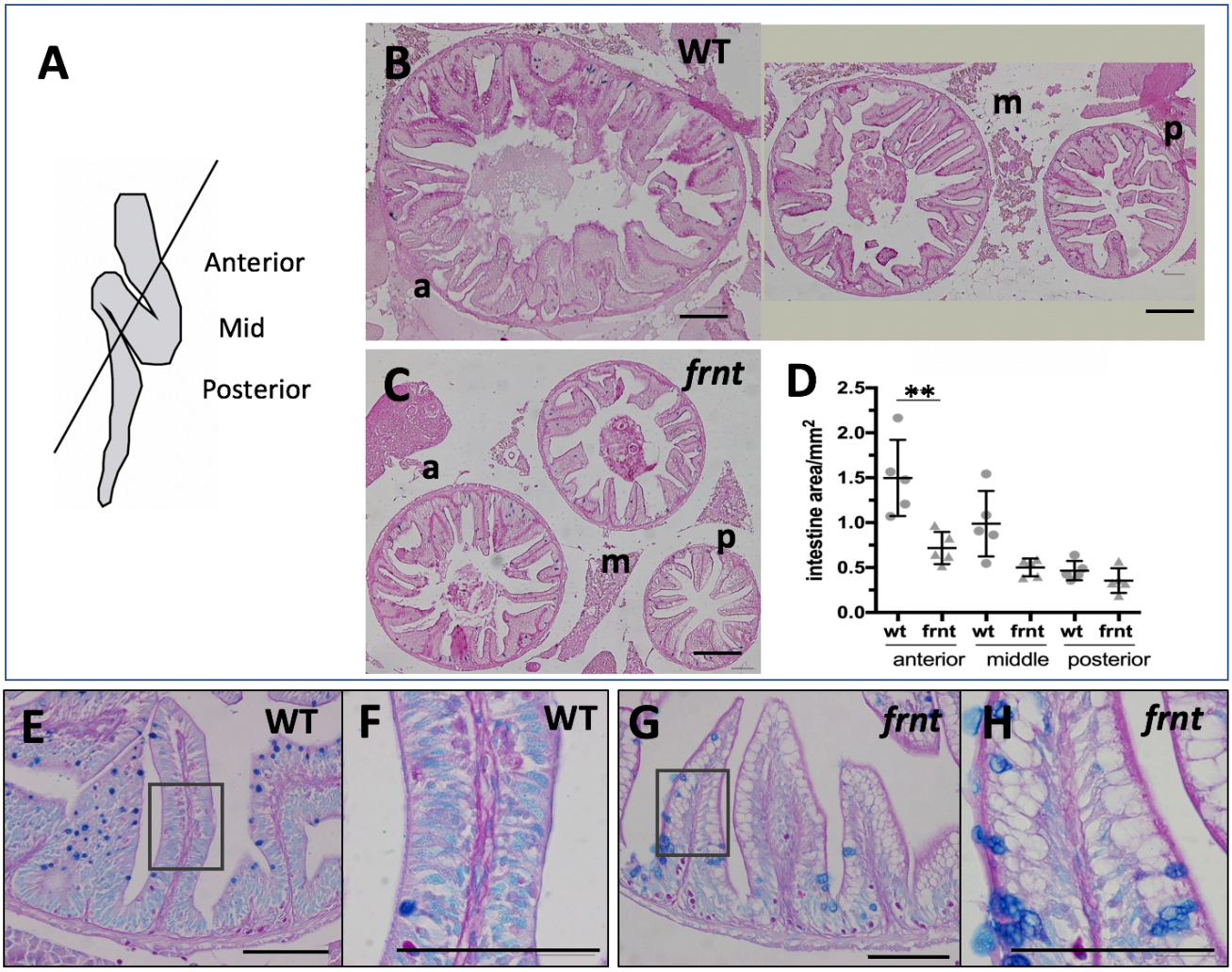

Supplementary Figure 2. *Celsr1a* affects intestine growth and homeostasis.

A) Schematic of adult zebrafish intestine showing plane of section demarcating anterior (a), middle (m), and posterior (p) domains of the intestine for analysis (after (Wallace et al., 2005)). **B**) Histomorphology of 6 month-old wild-type sibling (wt) adult intestine showing decreasing circumference along the length of the intestine and prominent rugae growing up into the intestinal lumen. **C)** Intestine of age and size matched *frnt* mutants. Sections stained with PAS. **D**) Quantitation of intestine area in different gut regions in wt sibling and *frnt* mutants; data represented as mean ± standard deviation, **p<0.01. **E-H**). PAS and Alcian blue staining of rugae from wt (E-F) and *frnt* mutant fish. Inset (E, G) showing area of F, H. Scale bars represent 100um.

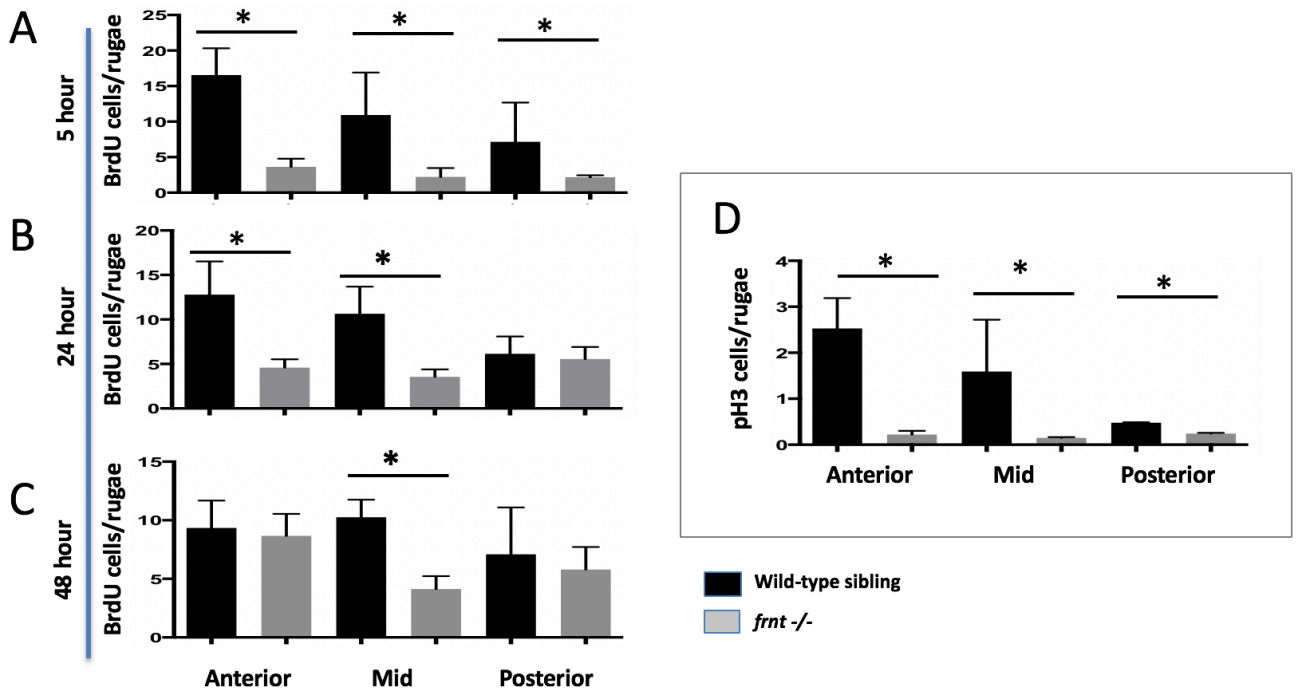

Supplementary Figure 3. Cell cycling is diminished in *celsr1a* mutant intestinal epithelia. **A-C**) Different lengths of chase after Bromodeoxyuridine (BrdU) treatment of 6 months-old *frn*t and wild-type (wt) control fish. **A**) 5 hours; **B**) 24 hours and **C**) 48 hours chase. **D**) Analysis of phospho-histone H3 (pH3). Measured number of positive cells per intestinal rugae from anterior, middle and posterior positions of the gut. 3-4 fish were used per treatment group. Data represented as mean ± standard deviation, *p<0.05.

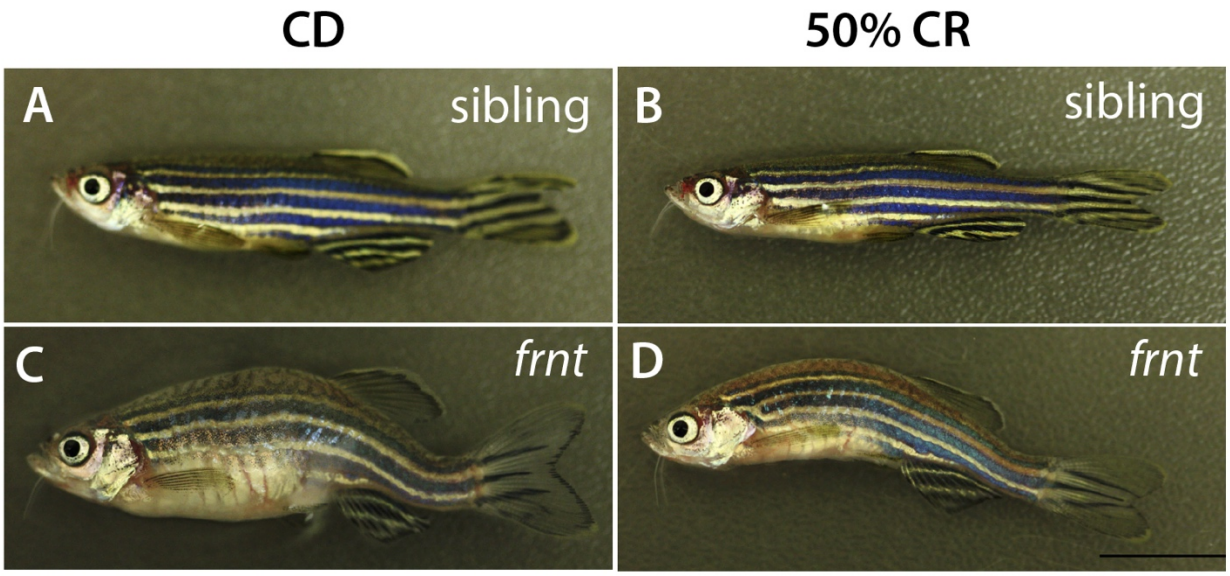

Supplementary Figure 4. Morphology of caloric restricted zebrafish. Representative adult fish after feeding regimen of control or calorie restricted (CR) diet. **A-B**) *frnt* siblings showing healthy outward appearance in control (**A**) or 50% CR groups (**B**). *frnt* mutants retained outward aging appearance after being fed a 50% caloric restricted diet (**D**) with comparable kyphosis and scale defects as seen in control treated animals (**C**).

Supplementary Movie 1.

Altered swimming behavior and response to acoustic stimuli in *celsr1a* mutants. Celsr1a mutants (pigmented) and wild-type albino fish respond to periodic tank tap as an acoustic stimulus.

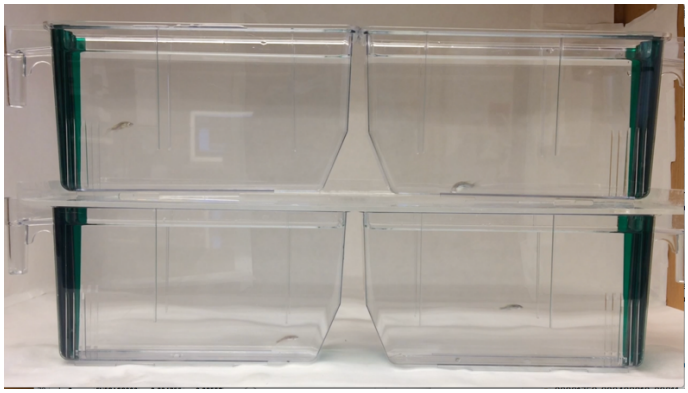

Supplementary Movie 2

Behavioral analysis of celsr1a mutant fish after raising in diets of different caloric content.

Supplementary table 1 : Defined diets for zebrafish dietary restriction.

	Control Diet (CD)		25% Caloric Reduction (CR)		50% Caloric Restriction	
Component	**% total**	**kcal**	**% total**	**kcal**	**% total**	**kcal**
Protein	49.5	181.9	37	136	19.7	72.392
Carbohydrate	26.5	95.4	13	46.8	5.3	19.08
Lipid	12	94.25	12	94.25	12	94.25
Fiber	3	-	29	0	54	0
Vitamins/Minerals	9	-	9	n/a	9	n/a
total		371.55		277.05 (75%)		185.72 (50%)

Recipe adjustments

Ingredient	**CD**	**25%CR**	**50%CR**
Wheat Gluten (g)	15	11	6
Casein (g)	30.5	23	12
Egg Whites (g)	4	3	1.7
Cellulose (g)	3	29	54
Starch (g)	26.5	13	5.3
Soybean Oil (g)	7	7	7
Ultralec lecithin (g)	5	5	5
Vitamin Mix (g)	4	4	4
Mineral Mix (g)	4	4	4
Stay C (g)	1	1	1
Total Weight (g)	100	100	100
Total Kcal (without vitamins & minerals)	371.55	279.05	186.55

Caloric content of ingredients

(derived from indicated company websites)

Ingredient	**Content**
Wheat Gluten (Dyets Inc. #402100)	3.56 kcal/g
Casein (Dyets Inc. #400627)	3.72 kcal/g

Egg Whites (Dyets Inc. #401600)	3.76 kcal/g
Cellulose (Dyets Inc. #401850)	-
Vitamin Mix (Dyets Inc. #310069)	-
Mineral Mix (Dyets Inc. #210087)	-
Stay C* (Vitamin C-3, Argent Chemical Laboratories Inc.)	-
Starch (Baka-Snak Food Starch-Modified, National Starch Food Innovation)	3.6 kcal/g
Lecithin (ADM, Ultralec without added tocopherol)	6.25 kcal/g
Water (Milli-Q)	-
Tocopherol stripped soybean oil (Dyets Inc. #404365)	~9.00 kcal/g
Vitamin E (Novatol 6-92, Archer Daniels Midland)	-
Total kcal per 100 g batch of control diet	371.55
Kcal/g of diet (not counting vit and mineral mixes)	4.22

Supplementary table 2: Primers used in the study.

primer name	Sequence (5'-3')	purpose
sox2-Fw	GCTCTGCACATGAAGGAACA	*in situ* hybridization
sox2-Rv	TTTCCCTCCCCAAAAGAAGT	
olfm4-Fw	GAGGTGATTCGCCATGAGTT	*in situ* hybridization
olfm4-Rv	AGCACCAAGACACTGCACAC	
celsr1a-qPCR-F	CAACCTACCACCTCCTTTCTTC	qRT-PCR
celsr1a-qPCR-R	CAGCCTTCACTAGGTTCTCATT	
celsr1b-qPCR-Fw2	GACGGGTGTAATGTACCTGATG	qRT-PCR
celsr1b-qPCR-Rv2	CACAGTCCCTGCCGAAATAA	
celsr2-Fw	CATTGCGTTTGTGGTGTCTATG	qRT-PCR
celsr2-Rv	TCTCTTCTCGCAGCTCTTCT	
celsr3-Fw	CCACTCAGAAGGAGATCAAGAAG	qRT-PCR
celsr3-Rv	CATCAGACCAAACAGCCAAAC	
sirt1-F	GTCCAATCAGCAAACGACTCGGAG	qRT-PCR
sirt1-R	TCTTCATGCTGGAAAGATCCGTCG	
sirt6-F3	GAGGACAGGACACCTCAAATAC	qRT-PCR
sirt6-R3	TGCCACACTTCTCACATTCT	
cdnk1a/p21-F	AGCTGAAGCGCAAACAGA	qRT-PCR
cdnk1a/p21-R	GTAGATGCAGGTCAAGAGTTTATCT	
pax7a-qPCR-Fw	GACACACTACCCTGACATCTAC	qRT-PCR
pax7a-qPCR-Rv	CCTTGCTCTTCTGTTGCTAAAC	
deltaNp63-Fw	GAGACCAATGCTCCCTCA	qRT-PCR
deltaNp63-Rv	GGCTGGTGGATGTGGAG	
cldnb-qPCR-Fw	ACAGATGCAGTGTAAGGTCTAC	qRT-PCR
cldnb-qPCR-Rv	ATTCCCATGACTCCGATCAC	